NASA TN D-694

# TECHNICAL NOTE

## D-694

MEASURED TWO-DIMENSIONAL DAMPING EFFECTIVENESS OF FUEL-SLOSHING BAFFLES APPLIED TO RING BAFFLES IN CYLINDRICAL TANKS

By Henry A. Cole, Jr., and Bruno J. Gambucci

Ames Research Center
Moffett Field, Calif.

NATIONAL AERONAUTICS AND SPACE ADMINISTRATION
WASHINGTON
February 1961

NATIONAL AERONAUTICS AND SPACE ADMINISTRATION

TECHNICAL NOTE D-694

# MEASURED TWO-DIMENSIONAL DAMPING EFFECTIVENESS OF FUEL-SLOSHING BAFFLES APPLIED TO RING BAFFLES IN CYLINDRICAL TANKS

By Henry A. Cole, Jr., and Bruno J. Gambucci

## SUMMARY

Measured two-dimensional damping forces of baffles with various shapes and perforations are presented for fluid conditions representative of those in liquid-fuel rocket vehicles. The effects of amplitude and frequency of fuel sloshing, and surface proximity on baffle damping are shown. Application of the results in the prediction of damping effectiveness of ring baffles in cylindrical tanks is demonstrated. Finally, some measurements of damping in a free-free cylindrical tank are presented which verify the predictions based on two-dimensional results. Measurements of certain three-dimensional baffles show that they provide greater damping than ring baffles.

## INTRODUCTION

The fundamental sloshing mode of a liquid propellant in a cylindrical tank is a problem of some concern in the stability and control of many rocket vehicles. This mode, which may be described as a pendulum-like motion in which the fluid sloshes from side to side, usually occurs at frequencies which are slightly higher than the natural frequency of the control system. Consequently, unless some damping is introduced into the liquid propellants, the oscillating forces of the sloshing fuel may cause the over-all dynamic system to become unstable. Usually the amount of damping required for stability is determined from analog studies. The remaining problem, then, is to find a baffle of minimum weight which gives the necessary amount of damping.

Fuel-sloshing baffles are usually designed by cut-and-try methods in ground oscillation tests of full-scale or model tanks. The difficulty in such tests is that the natural frequencies of the fluid in a tank on the ground are fixed, whereas the frequencies of the fluid in a rocket in flight increase with acceleration. Hence, it is not possible to exactly duplicate the fluid conditions in flight unless the ground test tank is also accelerated. Since this is not practical, frequency

effects are usually simulated by oscillation tests of scale models with various fluids. However, such tests are usually conducted for particular configurations and are not generally applicable.

Another technique for determination of damping uses strip theory. In this method the motion of the fluid is assumed to be the same as that given by analytical solutions for an inviscid fluid. The damping of individual radial strips is then calculated through use of the local velocity and two-dimensional damping characteristics. The total damping is then obtained by summing the damping of the individual strips. Predictions of ring damping in cylindrical tanks have been made by this method in reference 1 through use of the two-dimensional data in reference 2. Unfortunately, the latter data were limited to a single oscillating frequency and do not include surface-wave effects.



To provide damping data on the two-dimensional effectiveness of baffles over a range of frequencies, amplitudes, and fluid depths a special baffle tester was devised. The motion of fluid and baffle were interchanged, much as motion of air and model are interchanged in a wind tunnel (see fig. 1). In this device, the baffle is attached to a blade which is oscillated up and down at various frequencies and amplitudes. The natural modes of the fluid in the test tank are controlled by special plates on the liquid surface. In this way, frequency can be varied without changing the size of the test tank.

In the present report, the results of damping measurements on 27 baffle configurations in the two-dimensional tank are presented, and the important parameters which determine the damping effectiveness of a baffle are brought out. A method for prediction of damping effectiveness of baffles in cylindrical tanks, using the two-dimensional data, is developed. Then the damping principles are used in the design of several three-dimensional baffles which are more effective than ring baffles. Finally, damping measurements of a cylindrical tank suspended on cables are presented to verify the prediction method for ring baffles and to demonstrate the effectiveness of the three-dimensional baffles.

## NOTATION

| | |
|---|---|
| $A$ | baffle double amplitude, ft |
| $A_W$ | double amplitude of test tank first sloshing mode, ft |
| $C_D$ | drag coefficient (see eq. (6)) |
| $C_{D_O}$ | drag coefficient of flat plate used for comparison |
| $F$ | measured baffle force, lb |

| | |
|---|---|
| $R$ | Reynolds number, $2\pi \frac{\rho}{\mu} \frac{Aw}{T}$ |
| $S$ | baffle area, sq ft |
| $T$ | period of oscillation, sec |
| $a$ | cylindrical tank radius or one half length of rectangular tank |
| $a_1$ | amplitude of fundamental-frequency baffle force in phase with velocity, lb |
| $b_1$ | amplitude of fundamental-frequency baffle force $90^\circ$ out of phase with velocity, lb |
| $d$ | depth of baffle measured from quiescent liquid surface to mean position of outer edge of baffle, ft |
| $g$ | acceleration, $ft/sec^2$ |
| $h$ | depth of fluid, ft |
| $t$ | time, sec |
| $w$ | chord of baffle measured from wall along perpendicular line to outer edge of baffle, ft |
| $y$ | baffle position, positive downward, ft |
| $y_s$ | surface position, positive downward, ft |
| $\zeta$ | damping ratio |
| $\mu$ | viscosity, slugs/ft sec |
| $\rho$ | mass density, $slugs/ft^3$ |
| $\varphi$ | phase angle, deg |
| $\omega$ | frequency of forced oscillation, radians/sec |
| $\omega_n$ | natural frequency of fluid, radians/sec |

## TEST EQUIPMENT

### Two-Dimensional Tank

The test equipment for measurement of two-dimensional effectiveness of fuel-sloshing dampers is shown in figure 2. The up and down reciprocating motion indicated in figure 1 was approximated by rotary motion of the blade and baffle about the pivot point. The blade to which baffles were attached was curved to match the radius drawn from the pivot point. The radius was made as large as practical to keep rotation of the baffle small so that the principal motion would be translation. The beam supporting the blade was driven by a variable-speed drive which operated at frequencies of 0 to 3 cycles per second and amplitudes from 0 to 12 inches. Baffle depth was varied by changing the attachment point of the baffle segment on the blade. Heaters were installed in the bottom of the tank so that temperature, and hence viscosity, could be varied.



The blade was attached to the beam by three strain gages which were connected in parallel so that side forces of the fluid on the blade were canceled. Since the mass of the blade and baffle mounted on strain gages introduced inertial forces which were not wanted in the measurements, an accelerometer was included in the circuit to cancel the basic inertial output of the strain gages. Consequently, the output of the balance system was substantially proportional to the fluid forces on the baffle.

The test tank was 1×5×5 feet in size and was filled with water to the 4-foot level. The natural modes of the fluid were restrained by various surface wave devices shown in figure 3. The surface wave suppressor (fig. 3(a)) was a plate which completely restricted the surface except for small gaps around the sides. The surface wave damper (fig. 3(b)) was a perforated plate which dissipated traveling waves created by the baffle when the surface of liquid was free in the left side of the tank. Since the first natural mode of the liquid in the test tank was not completely damped by the wave damper, a float-type wave height gage was installed at the end of the tank to measure the response of the mode to be used in corrections to baffle motion. The baffles were also fitted with end plates (fig. 3(c)) to minimize gap losses between baffle and tank wall. Other instrumentation included a baffle position indicator and a recording oscillograph.

### Three-Dimensional Tank

Test equipment for measuring the three-dimensional effectiveness of fuel-sloshing dampers (shown in fig. 4) consisted of a 3-foot diameter tank suspended on 16-foot cables, a hydraulic drive with an automatic release mechanism, and heaters. Instrumentation consisted of resistance

type transducers for measuring the tank displacement and the location of a float on the liquid surface near the wall. A guide was installed at the bottom of the tank to maintain translational motion.

## MEASURED TWO-DIMENSIONAL BAFFLE DAMPING FORCES

Forces were measured on the configurations shown in figure 5. Flat plates were tested with chords of 3, 6, 9, and 12 inches. All other plates had 6-inch chords measured from the outer edge along the normal to the wall.

### Reduction of Data

A typical time history of a baffle test is shown in figure 6. Quantities recorded were baffle position, baffle force, and wave height at the wave damper. The travel of the float on the wave gage was limited by the wave damper; hence only positive wave motions were recorded. If baffle motion is considered positive downward and zero time taken at bottom dead center, then baffle motion is represented by

$$y = \frac{A}{2} \cos \omega t \tag{1}$$

The measured force was expanded into a Fourier series as follows:

$$F = a_1 \sin \omega t + b_1 \cos \omega t + \ldots \tag{2}$$

where

$$a_1 = \frac{\omega}{\pi} \int_0^{\frac{2\pi}{\omega}} F \sin \omega t \, dt \tag{3}$$

and

$$b_1 = \frac{\omega}{\pi} \int_0^{\frac{2\pi}{\omega}} F \cos \omega t \, dt \tag{4}$$

Only the fundamental frequency terms are needed because the higher frequency terms do not contribute to the damping.

The integrals (3) and (4) were evaluated by the quadrature method of Filon (ref. 3) for 18 time intervals per cycle. This number of intervals was selected so that a parabola passed through any three adjacent points would give a good approximation to the curve.

Since the first mode of the fluid in the tank was only lightly damped by the wave damper, the values of $A$, $a_1$, and $b_1$ were corrected for the measured wave response $A_w$ and $\varphi$ (fig. 6) as indicated in

sketch (a). The vector $y$ represents the motion of the baffle relative to the tank. The vector $Ae^{-1.57d/a}$ represents the fluid motion at the baffle location which is obtained by correcting the measured surface wave by potential theory (ref. 4). These two vectors are subtracted to give the corrected $y$ vector which represents the motion of the baffle relative to the fluid. In most cases the correction was small, but near the fundamental fluid natural frequency the correction was so alrge that the data were rejected.

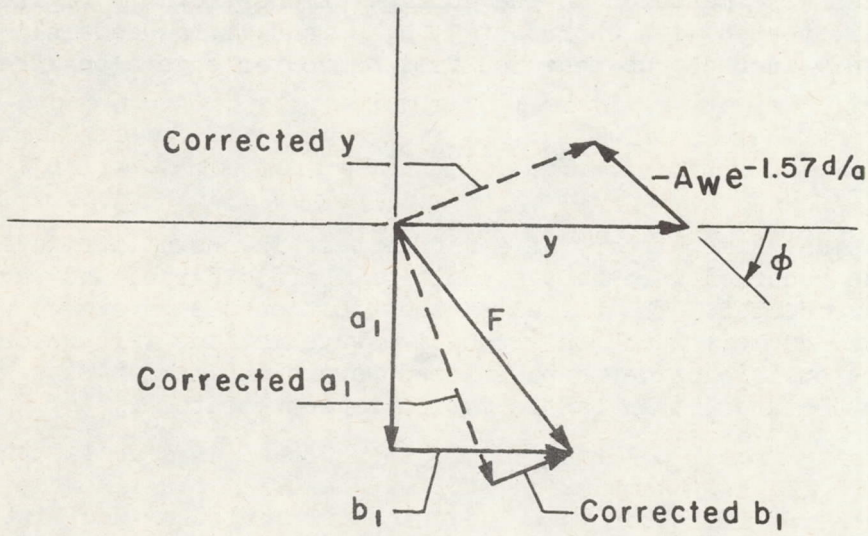


Sketch (a)

For purposes of comparison with results of references 1 and 2, the damping force was reduced to an equivalent drag coefficient as follows: Assume that the drag force is of the form

$$a_1 \sin \omega t = \frac{1}{2} \rho \left| \frac{dy}{dt} \right| \frac{dy}{dt} C_D S \tag{5}$$

To a first approximation from a Fourier series expansion

$$\left.\begin{aligned} |\sin \omega t| \sin \omega t &= \frac{8}{3\pi} \sin \omega t + \cdots \\ \text{so that} \qquad C_D &= \frac{3\pi a_1}{\rho S (A\omega)^2} \end{aligned}\right\} \tag{6}$$

It should be noted here that the use of an equivalent $C_D$ implies that the damping force is proportional to the velocity squared. Although this is not actually the case, the integral for $a_1$ is proportional to the energy dissipated in one cycle of oscillation. For this reason, even though the true form of damping forces may differ, the equivalent $C_D$ will give the correct rate of decay of the fluid.

The tare forces on the blade and end plates were the values measured without a baffle. Data obtained with baffles were only considered to be

valid when these tare forces were less than 10 percent of the measured force. Hence, the precision of the data in this report is ±10 percent.

Although the apparent mass forces ($b_1$) are not presented in this report, the values were determined and, in general, were less than the inertial force of the mass of fluid contained in a semicircular cylinder of radius w.

## Drag Coefficients of Flat Plate; Fluid Surface Suppressed

The surface plate was used to simulate the infinite depth condition of the baffle. Although the walls of the tank and the surface plate provide finite boundaries, the streamlines from potential flow are only distorted a few percent by a wall which is two chord widths or more from the baffle. Hence, the results obtained under these conditions are considered to be good approximations to those which would be obtained in a fluid of infinite extent.

Drag coefficients of plates with 3-, 6-, 9-, and 12-inch chords were obtained for amplitudes from 3 to 12 inches, frequencies up to 3 cycles per second, and temperatures from 70° to 212° Fahrenheit which change the viscosity from 1 to 0.284 centipoise. These data are plotted versus Aw/T in figure 7. Examination of time histories for like amplitudes and frequencies indicated that the viscosity variation had little effect. Consequently, drag coefficients were not computed for most of the elevated-temperature experiments, but a few points, the flagged symbols, are shown on the figure. It may be seen that the drag coefficients at the two temperatures agree within experimental errors and, consequently that Reynolds number could not be used as a scaling parameter. The curves also show that drag coefficient increases rapidly as the amplitude-to-chord ratio decreases, a result which is consistent with experiments reported in reference 2 on smaller plates. The experiments in reference 2 were limited to the area indicated in figure 7. It should be noted that a 3-inch plate in reference 2 would be equivalent to a 1-1/2-inch chord plate in this report because of the wall effect. Another trend noted in figure 7 is that drag coefficient rises as the chord of the baffle increases even though Aw/T and A/w are held constant.

In order to put the infinite-depth data in a form suitable for engineering use, a number of empirical equations were tried to fit the data. The most successful of these was an equation which consisted of the sum of three terms. The first term consisting of the velocity times the chord was included because the formation of small turbulent eddies was observed to occur at nearly the same velocity for all plates. The second term consisting of the velocity squared times the chord was included to account for the drag forces due to dynamic pressure. The third term consisting of the apparent mass force was included because it was noted that the force $b_1$ usually decreased relative to the theoretical apparent mass force whenever the drag force $a_1$ increased.

Since there was a possibility of some relationship or phase shift occurring in the apparent mass force due to drag, the term was included in the drag equation.

The drag-force equation, then was assumed to be of the form

$$a_1 = C_1 \frac{Aw}{T} + C_2 \frac{A^2w}{T^2} + C_3 \frac{Aw^2}{T^2} \qquad (7)$$

In coefficient form this becomes

$$C_D = 2.3 \frac{T}{A} + 3.6 + 2.4 \frac{w}{A} \qquad (8)$$

in which the constant values were obtained by fitting the curves of figure 7 by least squares. The accuracy of the fit is shown in figure 8.

Drag Coefficients of Flat Plate; Fluid Surface Free



Measured values of drag coefficient for various baffle depth ratios are shown in figures 9(a), 9(b), and 9(c) for the 6-, 9-, and 12-inch flat plates, respectively. At a frequency from 3 to 4 radians per second the surface effect becomes very large and the drag coefficient rises to a high value for all configurations. One might suspect that this resonant-appearing peak is due to the natural modes of the test tank, but, as mentioned in the section on Reduction of Data, the data were corrected for effects of the tank first sloshing mode. Also, the natural frequencies of the first two tank modes are indicated in figure 9(a), and it may be seen that they occur at higher frequencies than the drag coefficient peaks.

Observations on the fluid motion in the region of the high-drag peaks revealed a wave motion which was not unlike the action of waves breaking on a beach. On the downstroke, a surface wave would form and travel toward the wall and break into small eddies. See sketch (b). On the upstroke the wave would pile up at the baffle wall and then run out creating a turbulent shear layer as in sketch (c). This layer occurred at a low value of Aw/T (0.07 for 6-inch plate) which for oscillation well below the surface was a condition in which practically no turbulent eddies were observed.

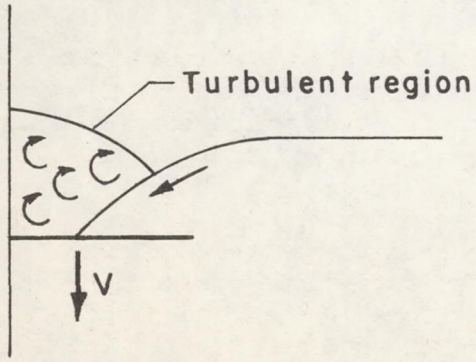


Sketch (b)

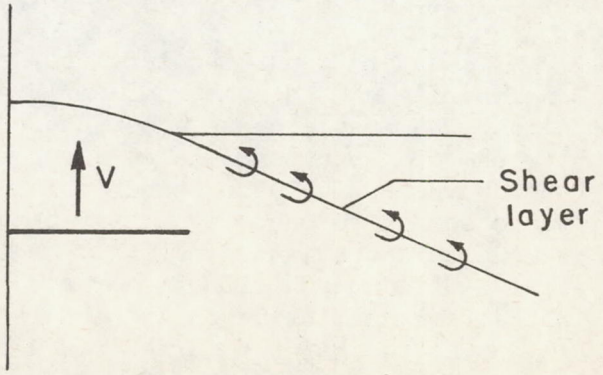


Sketch (c)

In figure 9 for the 6-inch, 9-inch, and 12-inch plates at amplitude-to-chord ratios of 1/2, 1/3, and 1/4, respectively, it may be seen that the peaks occur at about the same frequency. The amplitude is the same for each of these configurations which indicates that the high-drag region occurs at about the same velocity for all of the plates when the amplitude is small. When amplitude is increased from A/w of 1/2 to 1 on figure 9(a), much of the effect is lost, but the peak is shifted to a lower frequency, which also indicates that velocity of the baffle is the most important parameter.

Results were obtained for a 45° angled plate near the surface (fig. 9(a)) since such a configuration was reported by Bauer in reference 5. The plate tested was not perforated as in the reference, but was a solid plate with a projected chord of 6 inches. As seen in the figure the drag of this plate is even higher than the drag of the flat plate, a result which is believed to be due to the angled plate edge which creates additional resistance to the wave runout (sketch (d)).



For the wave motion mentioned above in connection with sketches (b), (c), and (d), it should be noted that the force out of phase with the velocity was 180° out of phase with the usual apparent mass force for infinite depth, thus indicating that the flow pattern was entirely different.

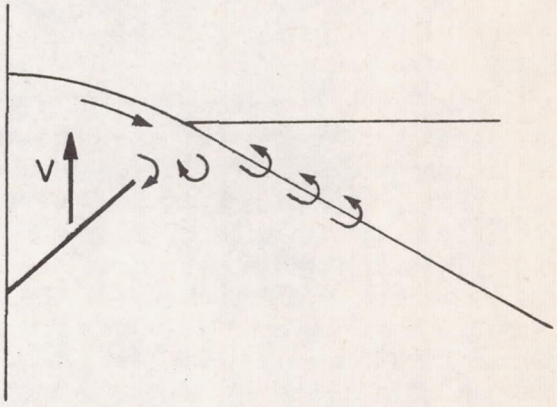


Sketch (d)

Above the critical velocity at which the special high-drag flow pattern developed, the drag coefficient dropped off rapidly with increasing frequency and even fell below the drag for infinite depth. This was caused by the formation of surface waves in the tank which traveled across the tank and were dissipated by the wave damper. For a study on traveling waves see Lamb, reference 4. The waves formed tend to reduce the effective amplitude of the baffle and hence reduce its effectiveness. For this type of motion little turbulence is formed and the apparent mass forces have the usual sign for infinite depth, thus indicating that the flow conditions are of the same nature.

## Effect of Perforating Plates

The possibility of saving weight by perforating baffles without reducing effectiveness was explored. The first series of tests was made on a 6-inch plate with a 1-inch lip. Two holes were cut in the plate

(fig. 5) with cutout area varied from 9.1 to 28 percent of total area. Figure 10 shows the ratio of drag coefficient of the baffle with cutouts, $C_D$, to drag coefficient of the baffle without cutouts, $C_{D_o}$. For small amplitudes ($A/w = 1/2$) and cutout areas up to 20 percent, the drag coefficient is not affected very much by the cutouts. However, for larger amplitude-to-chord ratios, the drag coefficient is less for all conditions.

Another series of tests was made in which the percent cutout area was held constant and the hole size was varied. Here again for low amplitudes the drag of the perforated plate was, at best, just equal to that of the baffle without cutouts. Perhaps the hole size was not small enough, but the results did not look encouraging and one can only conclude from these results that a perforated baffle will, at best, be just equal in effectiveness to a nonperforated one. Of course, if one compares a perforated plate and solid plate of equal areas, the perforated plate does recover some of the loss by virtue of its wider chord and, hence, lower amplitude-to-width ratio.



## Effect of Shaping Plates

Oftentimes various shaped plates, such as hat sections, lips, T, sandwich, and so forth, are considered to prevent undue deflections under sloshing loads. In order to investigate some of these configurations, the baffles shown in figure 5 were tested. The tests on these plates were for depth ratios of 2 or more, with the exception of the plate angled $45^\circ$ up, which was tested near the surface to correlate with the results of reference 5. A summary of the ratio of drag coefficients of above baffles to drag coefficients of a flat plate of equal chord width is shown on figure 11. At best, the plates were just equal in effectiveness to the flat plate at depth-to-chord ratio greater than 2. It appears that anything which is done to reduce the sharpness of the plate edge (lip, sandwich, T, etc.) reduces the baffle effectiveness, especially as $Aw/T$ becomes small. This supports the view that the development of turbulence is more dependent on the velocity of the fluid around the edge than the Reynolds number based on plate width. Configurations such as fingers and vanes are not very effective for oscillating flow, probably because the effective amplitude-to-width ratio is raised.

The unusually high effectiveness of the plate angled $45^\circ$ up near the surface ($d/w = 1/2$) is also indicated in figure 11. However, at greater depths it is noted that the angled plate was not as effective as the flat plate. Referring back to figure 9, one may see that for this critical region near the surface, the flat plate experienced a considerable increase in effectiveness when the depth ratio was changed from 1/2 to 1/4 and that the drag coefficients reached are as high as those for the angled plate. The angled plate, then, reaches the high value of drag coefficient farther from the surface than the flat plate.

On the basis of these results, it can be concluded that for depths greater than two chord widths, configurations in which the outer edge of the baffle is blunted tend to be less effective than a flat plate. Near the surface and below the critical velocity, the angled plate reaches the peak drag coefficients sooner than the flat plate as the mean oscillation depth approaches the surface.

## PREDICTION OF DAMPING IN CYLINDRICAL TANKS



The application of two-dimensional drag data to the prediction of damping in a cylindrical tank requires that the damping be small so that the velocities of the fluid may be predicted by potential flow theory of reference 4. Assume that the fluid is oscillating in the first sloshing mode only, and that this can be represented by a forced single-degree-of-freedom system:

$$m \frac{d^2y}{dt^2} + b \frac{dy}{dt} + ky = -F \sin \omega_n t \tag{9}$$

where m, b, k, and F are generalized mass, damping coefficient, spring constant, and force, respectively, and the dependent variable y now refers to the motion of the fluid at the baffle location. Using notation $\omega_n = \sqrt{k/m}$ and $\zeta = b/2m\omega_n$ and substituting $y = (A/2)\cos \omega_n t$ into equation (9), one obtains

$$\zeta = \frac{F}{mA\omega_n^2} \tag{10}$$

The potential energy of the liquid is from reference 4.

$$\text{P.E.} = \frac{1}{4} \rho g \pi a^2 \left[1 - (ka)^{-2}\right] \left(\frac{y_s}{y}\right)^2 y^2 \tag{11}$$

where $y_s$ is the displacement of the liquid surface and $ka = 1.84$.

Equating maximum potential and kinetic energies in the oscillation

$$\text{P.E.}_{max} = \frac{1}{2} m\omega_n^2 \left(\frac{A}{2}\right)^2$$

and solving for m, one obtains the generalized mass

$$m = \frac{\frac{1}{2} \rho g \pi a^2 \left[1 - (ka)^{-2}\right] \left(\frac{y_s}{y}\right)^2}{\omega_n^2}$$

and substituting in equation (10), one obtains the damping ratio

$$\zeta = \frac{2F\left(\frac{y}{y_s}\right)^2}{A\rho g\pi a^2\left[1 - (ka)^{-2}\right]} \qquad (12)$$

This equation expresses the relationship between the generalized force required to drive the mode at constant amplitude and the damping ratio. The force required to drive the baffle was expressed in terms of $C_D$ in equation (5). According to reference 4, the velocity around the periphery of the cylindrical tank varies as the $\cos\theta$. The generalized force then is given by the work done in a virtual displacement of $y$ which may be obtained by integrating the force around the cylinder

$$F\,\Delta y = 4\int_0^{\pi/2} C_D\,\frac{4}{3\pi}\,\rho\left(\omega_n\,\frac{A}{2}\cos\theta\right)^2 \Delta y\cos\theta\left(aw - \frac{w^2}{2}\right)d\theta$$



If $C_D$ is considered constant around the ring, then integrating above and substituting in equation (12), one obtains:

$$\zeta = \frac{16\,C_D\omega_n^2 A\left(aw - \frac{w^2}{2}\right)\left(\frac{y}{y_s}\right)^2}{9\pi^2 g a^2(0.704)} \qquad (13)$$

where

$$\frac{y}{y_s} = \frac{\sinh kh}{\sinh k(h-d)} \doteq e^{-1.84\ d/a}$$

and

$$\omega_n^2 \doteq \frac{1.84\ g}{a}$$

and in which $C_D$ is selected for the $A/w$ and $d/w$ ratios which occur at the baffle location. Since Reynolds number as defined here does not correlate the drag coefficients at various viscosities, it is recommended that $C_D$ be calculated from equation (8). It should be noted that $A$ is calculated by multiplying the surface double amplitude by $y/y_s$. Surface corrections can then be applied by interpolating the data of figure 9 to find a ratio of $C_D$ at the appropriate $\omega$, $d/w$, and $A/w$ to the $C_D$ for infinite depth. To be strictly correct, the $C_D$ function should be integrated around the ring, but the value of $C_D$ for the maximum liquid amplitude gives conservative results.

The correlation of damping predicted in cylindrical tanks by equation (13) with damping measured in cylindrical tanks is shown in figure 12. The tank diameters were 3 and 8.75 feet which correspond to natural frequencies of 6.3 and 3.6 radians per second, respectively. The $\zeta_{meas}$ for the 45° perforated ring near the surface was obtained by averaging the values from forced oscillation tests obtained in reference 5. The $\zeta_{meas}$ for a frequency of 6.3 was obtained from measurements of decaying oscillations in the 3-foot tank described elsewhere in this report. The $\zeta_{pred}$ for the 45° perforated ring was obtained through use of the measured drag coefficient (angled plate 45° up on fig. 9(a)) and a correction for the effect of 25-percent perforation determined from figure 10. The calculation is as follows:



Given:

$2y_s = 0.33$ ft (double surface amplitude)
$w = 0.58$ ft
$d = 0.25$ ft
$a = 4.38$ ft
$T = 1.75$ sec
$\omega_n = 3.6$

then:

$$y/y_s = e^{-1.84\ 0.25/4.38} = 0.9$$

$$A = (0.33)(0.9) = 0.3$$

$$\frac{A}{w} = 0.5,\ \frac{Aw}{T} = 0.1,\ \frac{d}{w} = 0.4$$

$C_D = 77$ (fig. 9(a))

Less 45 percent for perforations
(20 percent from fig. 10 plus
25 percent for area reduction)

Then from equation (13) $\zeta = 0.13$ and since the test tank had a measured 0.03 damping ratio due to tank formers,

$$\zeta_{pred} = 0.13 + 0.03 = 0.16$$

The $\zeta_{pred}$ for the ring baffles in the 3-foot tank was obtained through use of equation (8) and estimates of surface effects from figure 9. The calculation for the 3-inch ring follows:

Given:

$$2y_s = 0.25$$
$$w = 0.25$$
$$d = 0.625$$
$$a = 1.5$$
$$T = 1$$
$$\omega_n = 6.3$$

then:

$$\frac{y}{y_s} = 0.46$$

$$A = 0.115$$

$$\frac{A}{w} = 0.5, \quad \frac{d}{w} = 2.5, \quad \frac{Aw}{T} = 0.03$$



The value of $C_D$ calculated from equation (8) is 28.8 and, from figure 9(a), the surface correction is estimated to be 0.8. Then from equation (13) $\zeta_{pred} = 0.027$. No correction need be applied for the basic tank here because the measured two-dimensional data include drag of a smooth tank wall.

The cylindrical tank data show a satisfactory correlation with the predictions by two-dimensional tank data. Although there appears to be a tendency to overestimate the damping in the 3-foot tank, it should be noted that equation (8) does overestimate the $C_D$ of 3-inch chord plates (fig. 8) and, hence better correlation would be obtained if the measured two-dimensional drag coefficients were used. The use of equation (8) to obtain drag coefficients for baffle chords less than 3 inches is questionable.

## MEASURED THREE-DIMENSIONAL BAFFLE DAMPING EFFECTIVENESS

The cylindrical tank described in the section on test equipment was used to evaluate several baffles for which the flow could not be represented as two-dimensional. Baffles tested are shown in figure 13. The first of these was a 1-1/2-inch ring which was tested for a standard of comparison. The second one consisted of four semicircular plates placed at 90° intervals around the tank. The third type consisted of swirl plates which transform the first sloshing mode into rotary motion.

The procedure for measuring damping was to drive the tank in translation at its natural frequency until the desired wave amplitude was reached. A preset switch would then release the hydraulic drive so that

the tank was free to oscillate. The time histories of decaying oscillations of the surface wave were then analyzed for the logarithmic decrement which was then converted to damping ratio.

The results of damping measurements are shown in figure 14. All three baffles had the same projected area and were 1/16 inch thick. For the 9-inch depth, all plates had about the same effectiveness. However, near the surface, the swirl plates and the semicircular plates were more effective. Observations indicated that this was due to transformation of the first sloshing mode into other modes. The semicircular plates induced checkerboard surface waves with many distinct peaks, and the swirl plates introduced a rotary motion into the fluid. This transformation of energy appears as a loss of energy in the first sloshing mode, that is, higher damping. It should be noted that the swirl plates impart a rotary motion to the fluid only if the tank is roll stabilized. In the tests, the tank was restrained in roll by guides. If such an installation were used in a missile, the coupling of the sloshing mode to the roll control would have to be considered.

A 4 1 6

## EFFECT OF VISCOSITY ON DAMPING

Since all of the above tests were conducted with water, the question arises, how can the data be applied to other liquids? To check the effect of viscosity investigated in the two-dimensional tests, damping of the 1-1/2-inch ring was also measured at temperatures ranging from 70° to 212° Fahrenheit which corresponds to a viscosity change from 1 to 0.284 centipoise. For comparison, liquid oxygen has a viscosity of 0.189 centipoise at -183° centigrade. As shown in figure 15, there is little variation in damping below a depth of 4 inches when temperature is increased, that is, as viscosity is decreased. The data for baffle depths less than 4 inches indicated greater damping for the lower viscosity, but the results are not conclusive because of the amount of scatter. Apparently, when viscosity reaches a low level, it has little effect on the damping forces. If turbulent eddies are shed in such a way that they cannot be recovered on the successive cycle of motion, the same amount of energy is lost for one viscosity as for the other. Hence, it would appear that in the application of damping measurements in this report to fluids of lower viscosity, viscosity effects should be ignored by calculating drag coefficients from equation (8).

## CONCLUSIONS

The evaluation of force measurements from forced oscillation of 27 baffle configurations in a two-dimensional tank and damping measurements of ring baffles in a cylindrical tank has led to the following conclusions.

1. The damping effectiveness of ring baffles in cylindrical tanks can be adequately predicted from force measurements in a two-dimensional tank, even when surface effects are large.

2. The surface effects can be extremely large and should be taken into account for accurate prediction of damping.

3. For baffle depths greater than two chords, it appears that a flat plate with a sharp edge is the most effective damper. Changes in chordwise shape, baffle thickness, and perforations generally tend to reduce baffle damping effectiveness.

4. For baffle depths less than two chords, two widely different types of fluid damping occur separated by a critical velocity. Below the critical velocity, a traveling wave forms which breaks and creates turbulent shear layers and very high damping. Above the critical velocity, a smooth standing wave forms which reduces the effective motion of the baffle and, hence, its damping effectiveness.



5. To maximize damping effectiveness, the amplitude-to-chord ratio should be kept as small as possible.

6. For baffle depths of less than one chord width and below the critical velocity, plates which are angled up are more effective than flat plates.

7. Damping effectiveness is relatively independent of viscosity for water at viscosities from 1 to 0.284 centipoise.

For oscillations near the surface, semicircular plates and swirl baffles are more effective dampers than ring baffles because they transfer energy from the first sloshing mode into a high frequency "checkerboard" mode and a rotary mode, respectively.

Ames Research Center
National Aeronautics and Space Administration
Moffett Field, Calif., Dec. 13, 1960

## REFERENCES

1. Miles, J. W.: Ring Damping of Free Surface Oscillations in a Circular Tank. Jour. Appl. Mech., vol. 25, no. 2, June 1958, pp. 274-276.

2. Keulegan, Garbis H., and Carpenter, Lloyd H.: Forces on Cylinders and Plates in an Oscillating Fluid. National Bureau of Standards Rep. 4821, Sept. 5, 1956.

3. Filon, L. N. G.: Proc. Roy. Soc. Edin., XLIX 1928-1929, pp. 38-47.

4. Lamb, Sir Horace: Hydrodynamics, Sixth Ed., Dover Pub.

5. Bauer, Helmut F.: Fluid Oscillation in a Cylindrical Tank with Damping. Rep. DA-TR-4-58, Apr. 1958.

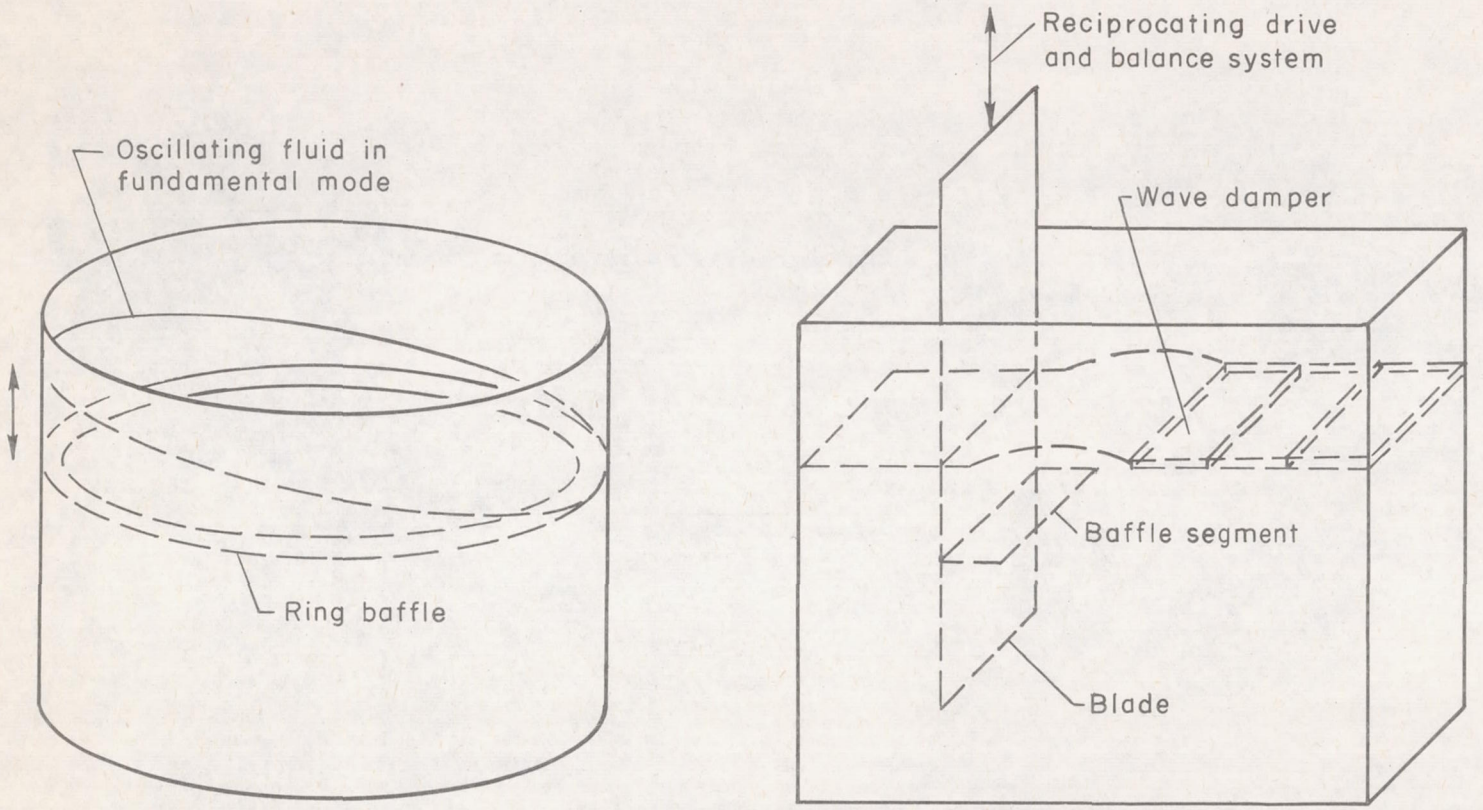


Cylindrical Tank

Variables { Amplitude, Baffle depth

Constant frequency

Two-Dimensional Tank

Variables { Frequency, Amplitude, Baffle depth

Figure 1.- Principle of fuel sloshing tests.

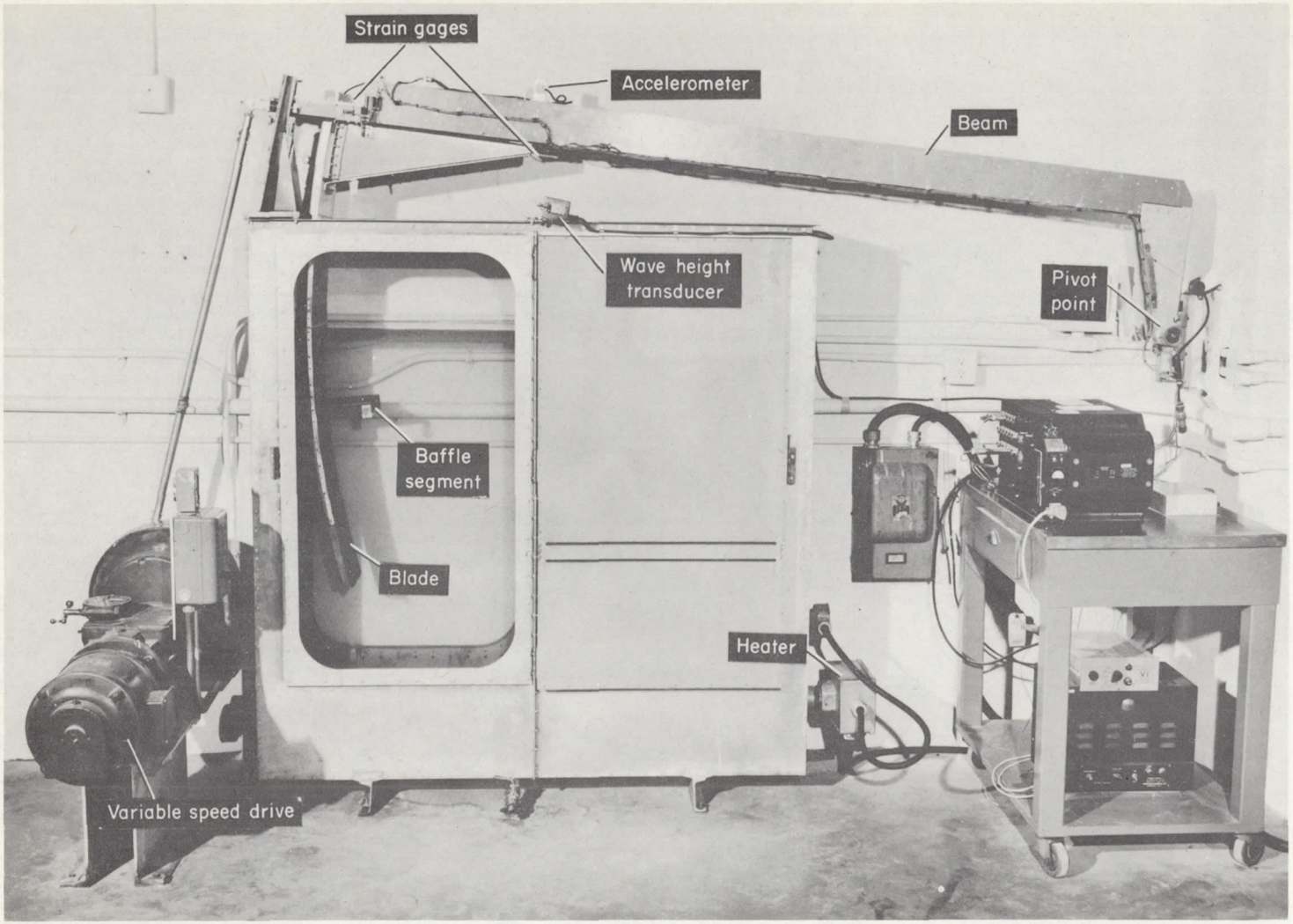


A-26943.1

Figure 2.- Front view of test equipment.

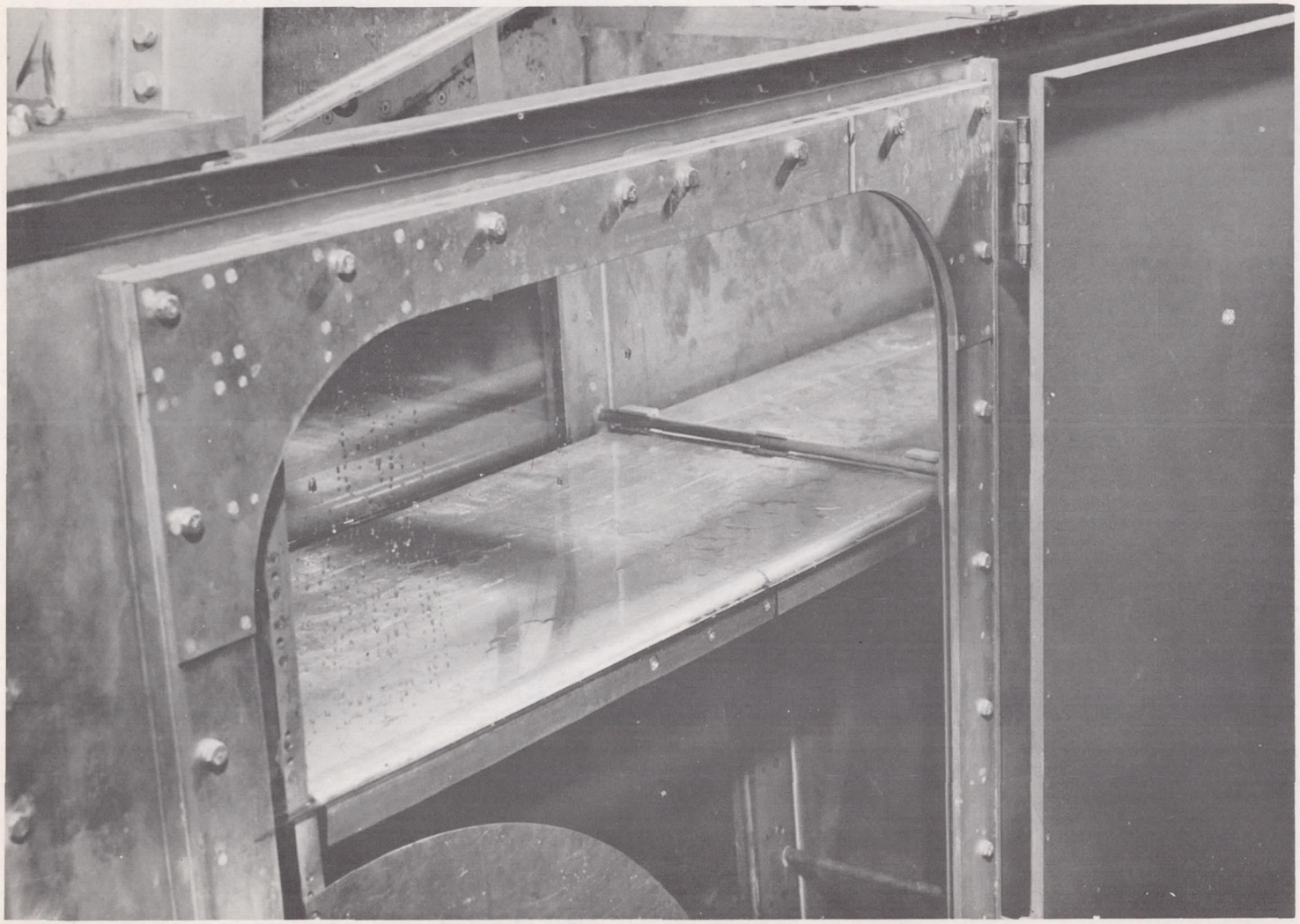

(a) Surface wave suppressor. A-26279

Figure 3.- View of surface wave control devices.

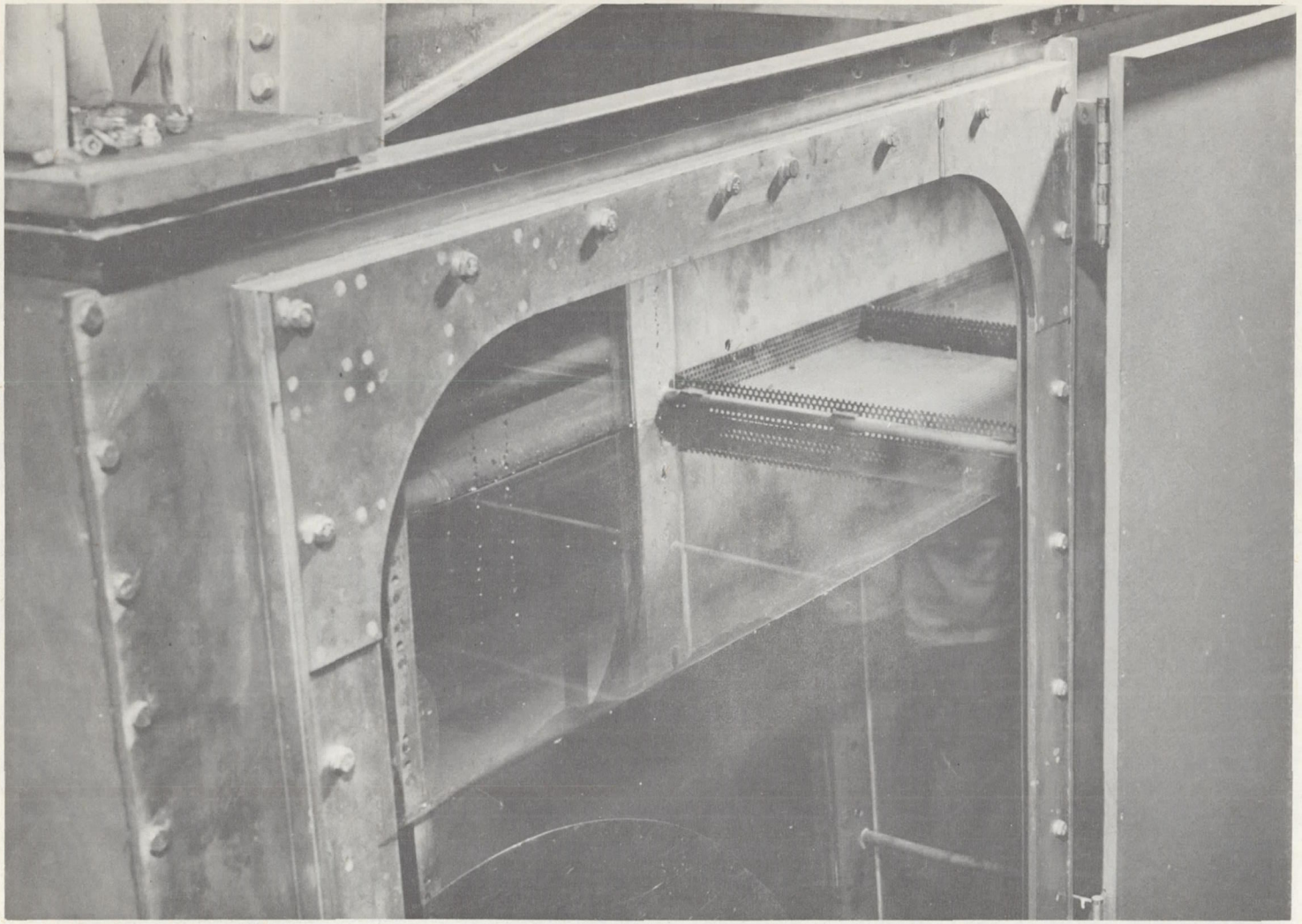

(b) Surface wave damper. A-26278

Figure 3.- Continued.

(c) End plates. A-26280

Figure 3.- Concluded.

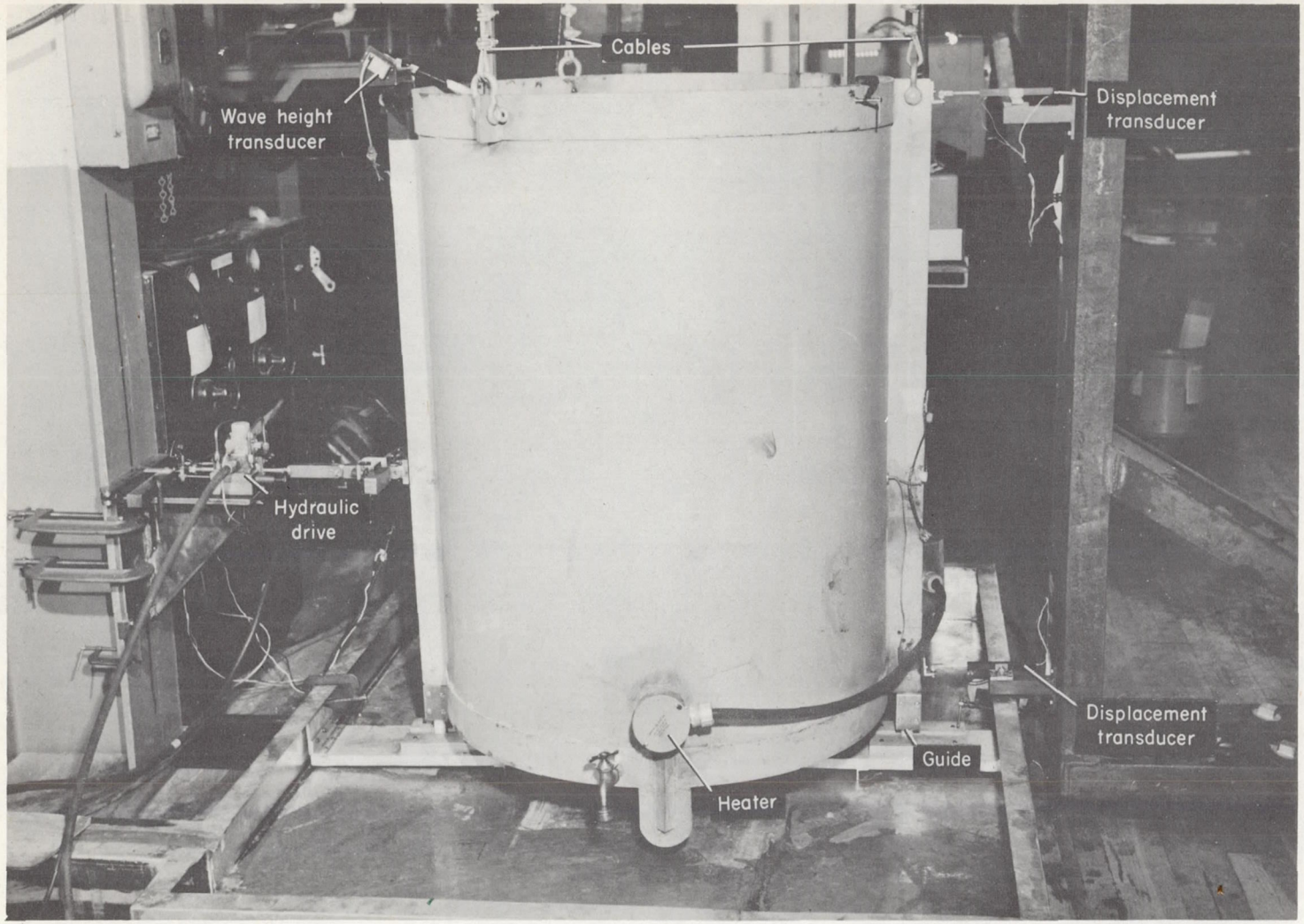


A-26504.1

Figure 4.- Photograph of free-free cylindrical tank.

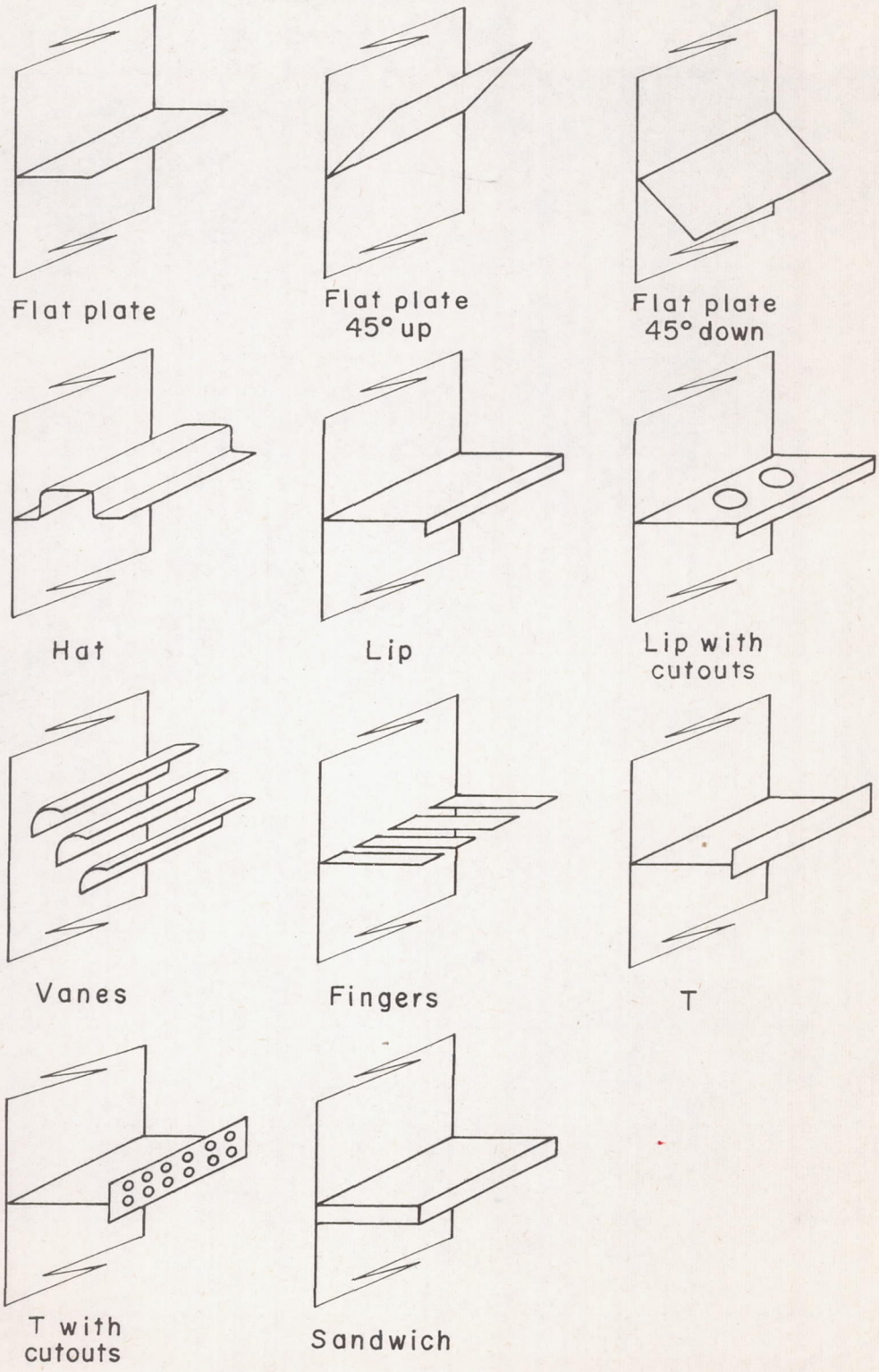


Figure 5.- Baffle configurations.

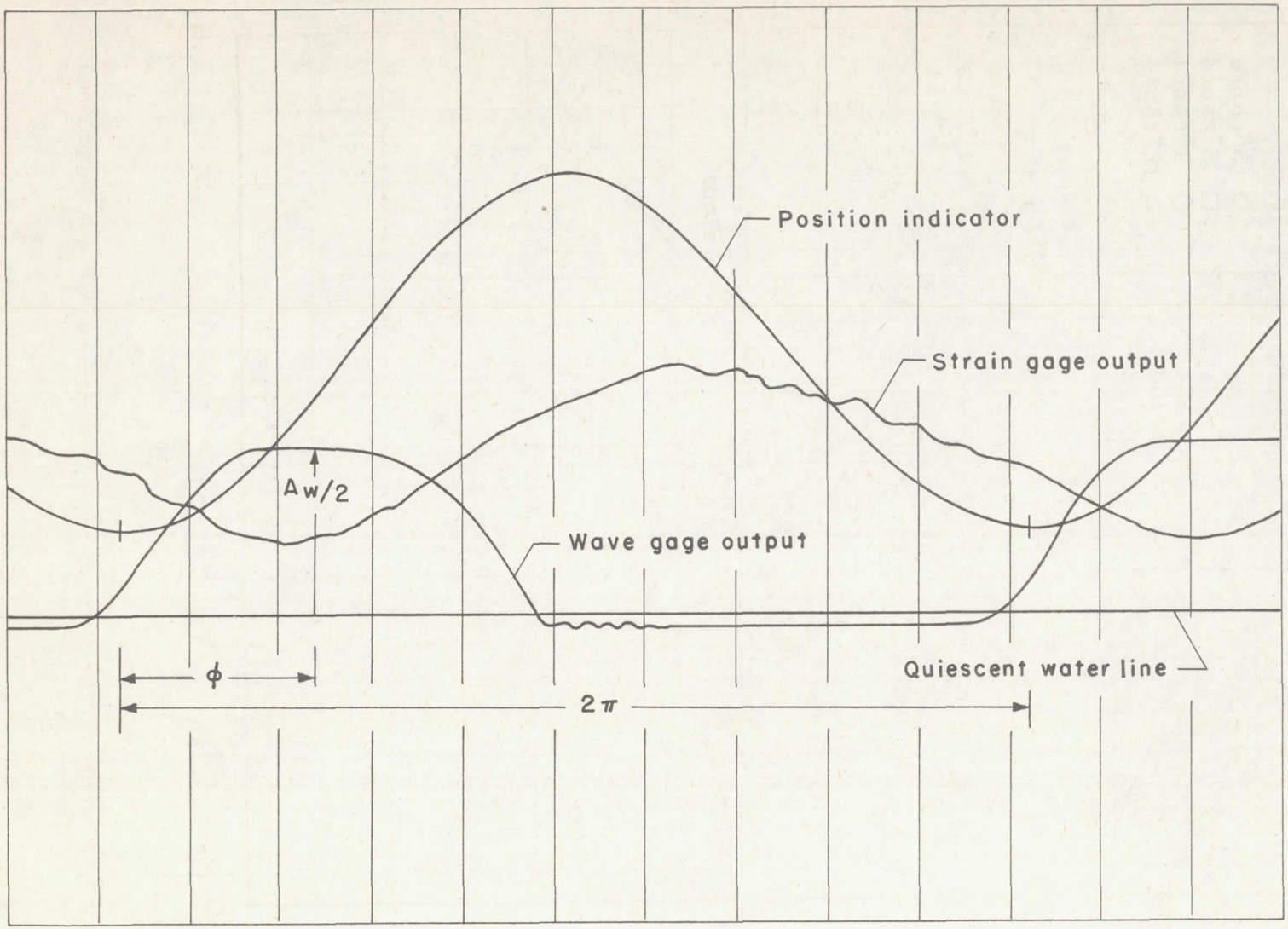


Figure 6.- Typical time history.

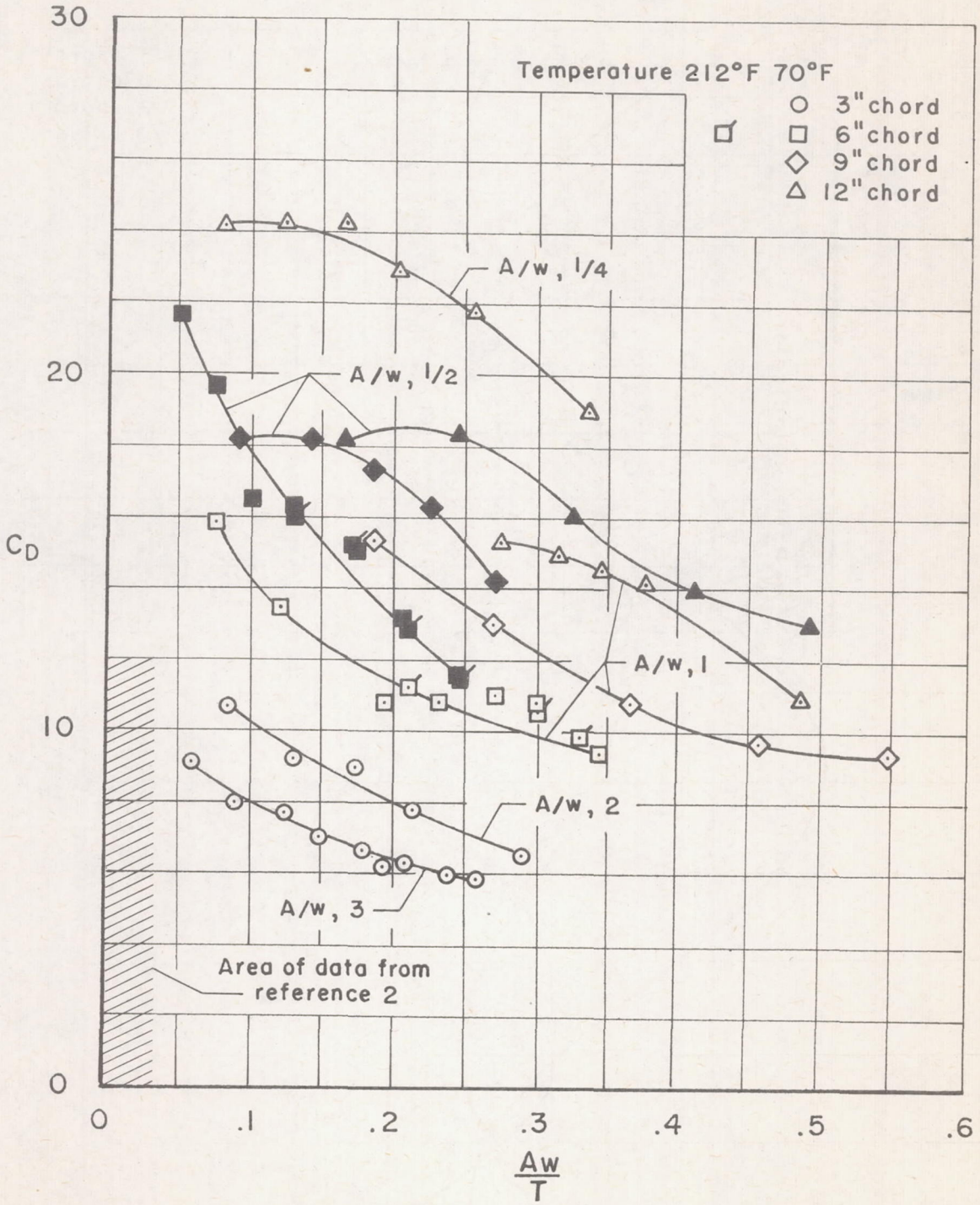


Figure 7.- Drag coefficient of flat plates with surface suppressed.

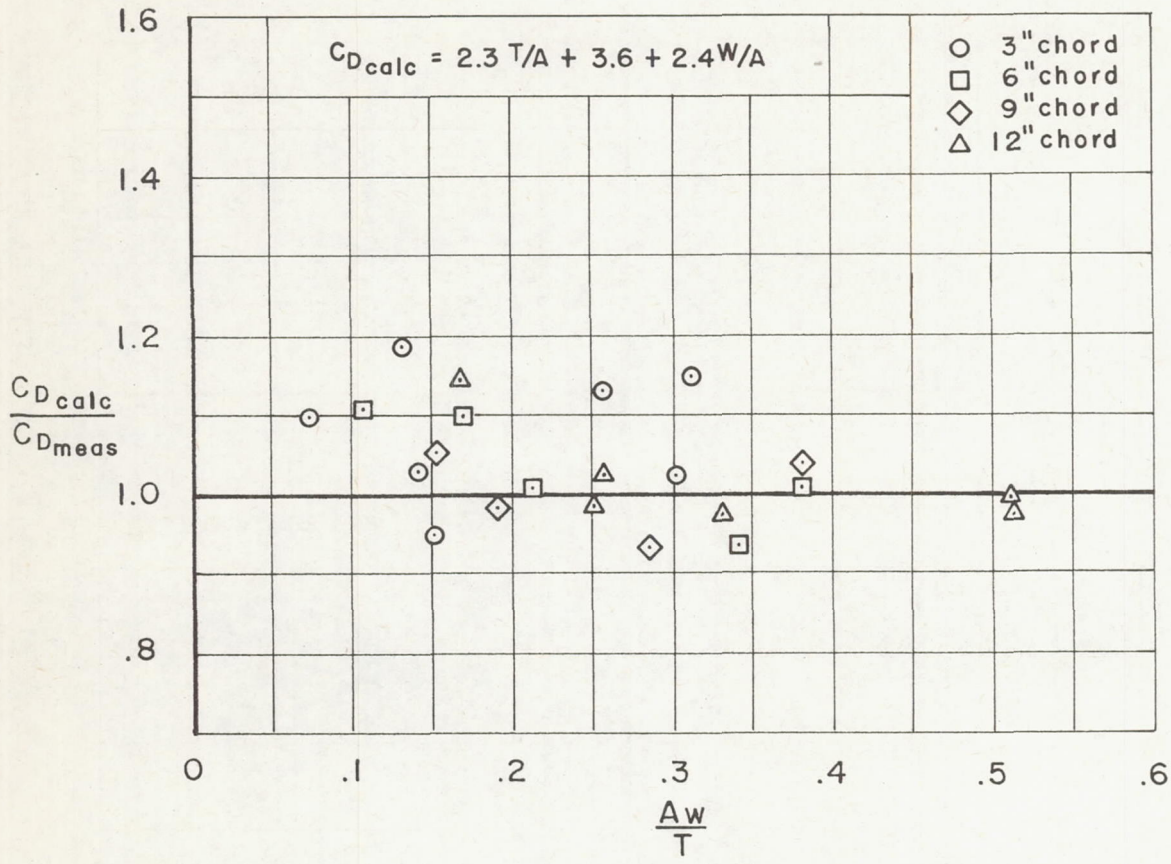


Figure 8.- Comparison of calculated and measured drag coefficients.

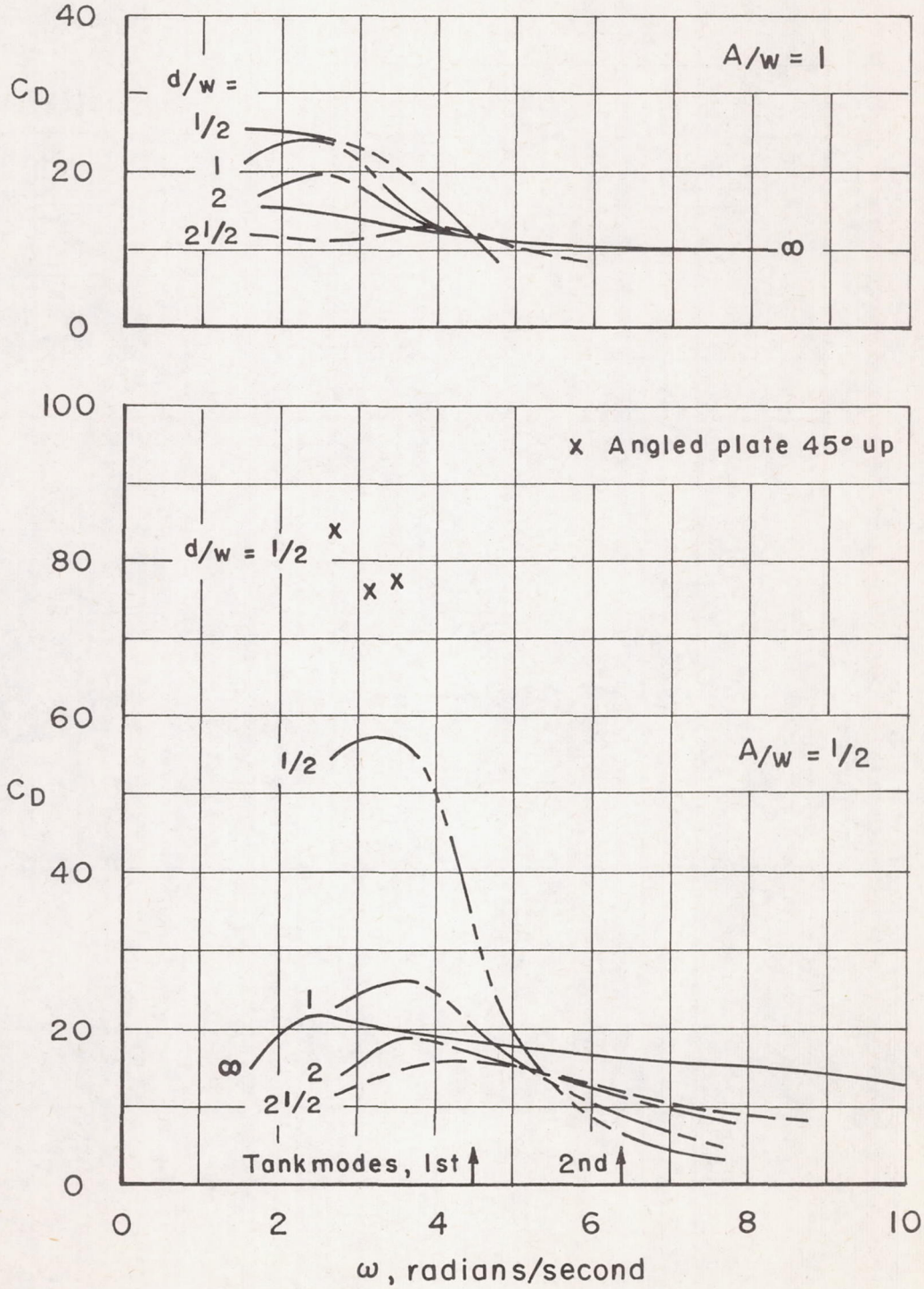


(a) 6-inch flat plate.

Figure 9.- Drag coefficient at several amplitudes and various depths.

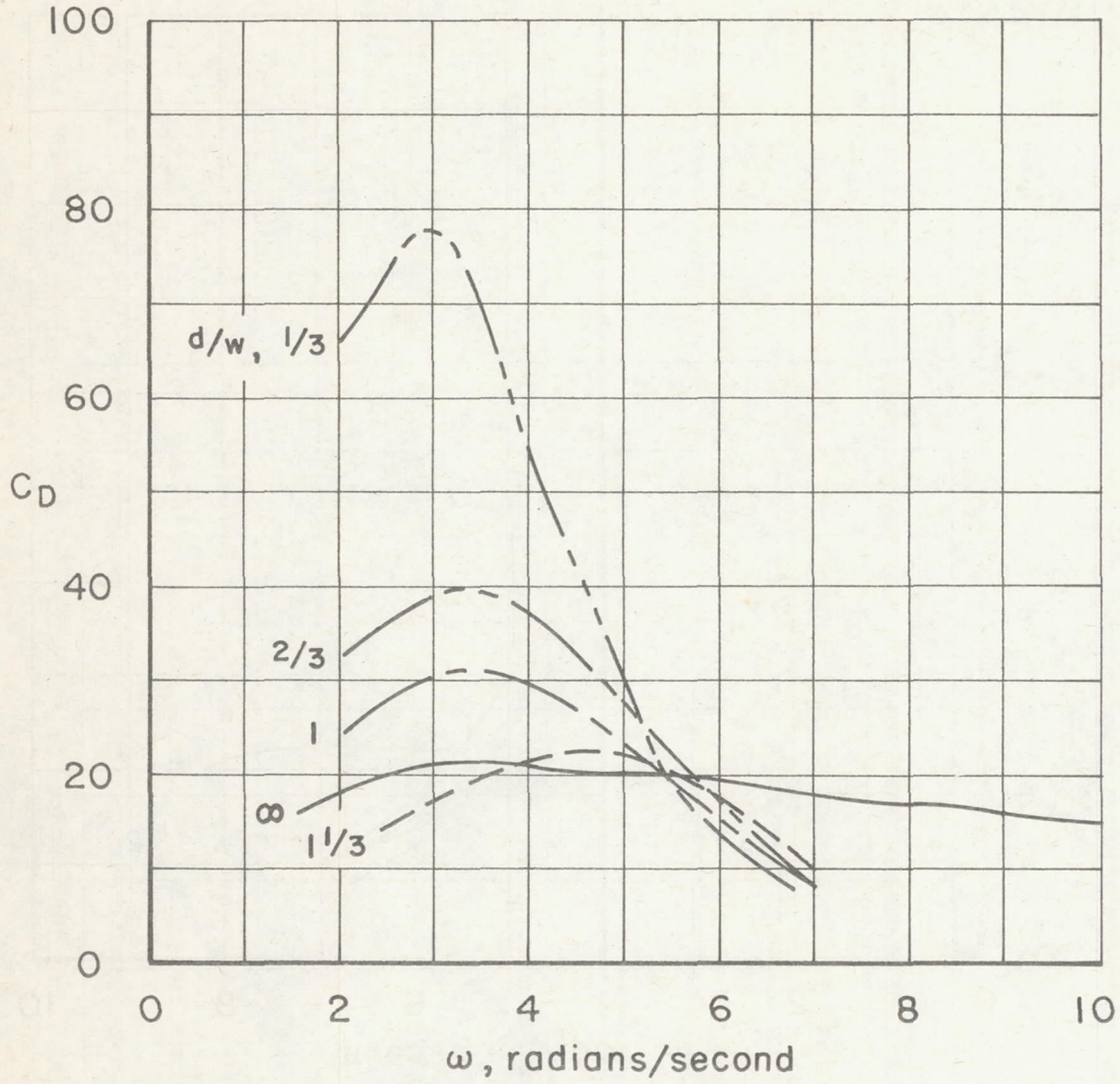


(b) 9-inch flat plate, $\frac{A}{w} = \frac{1}{3}$.

Figure 9.- Continued.

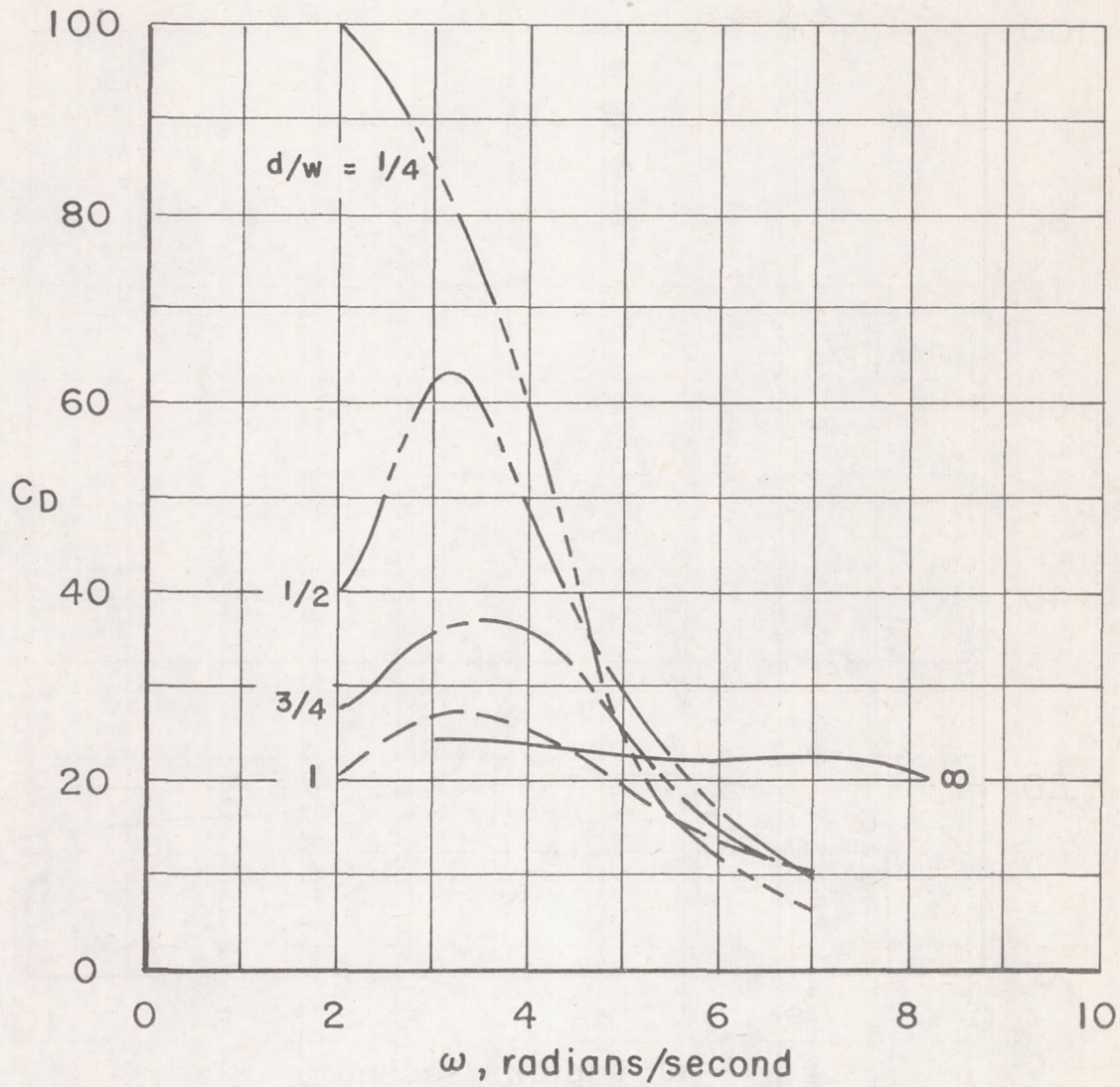


(c) 12-inch flat plate, $\frac{A}{w} = \frac{1}{4}$.

Figure 9.- Concluded.

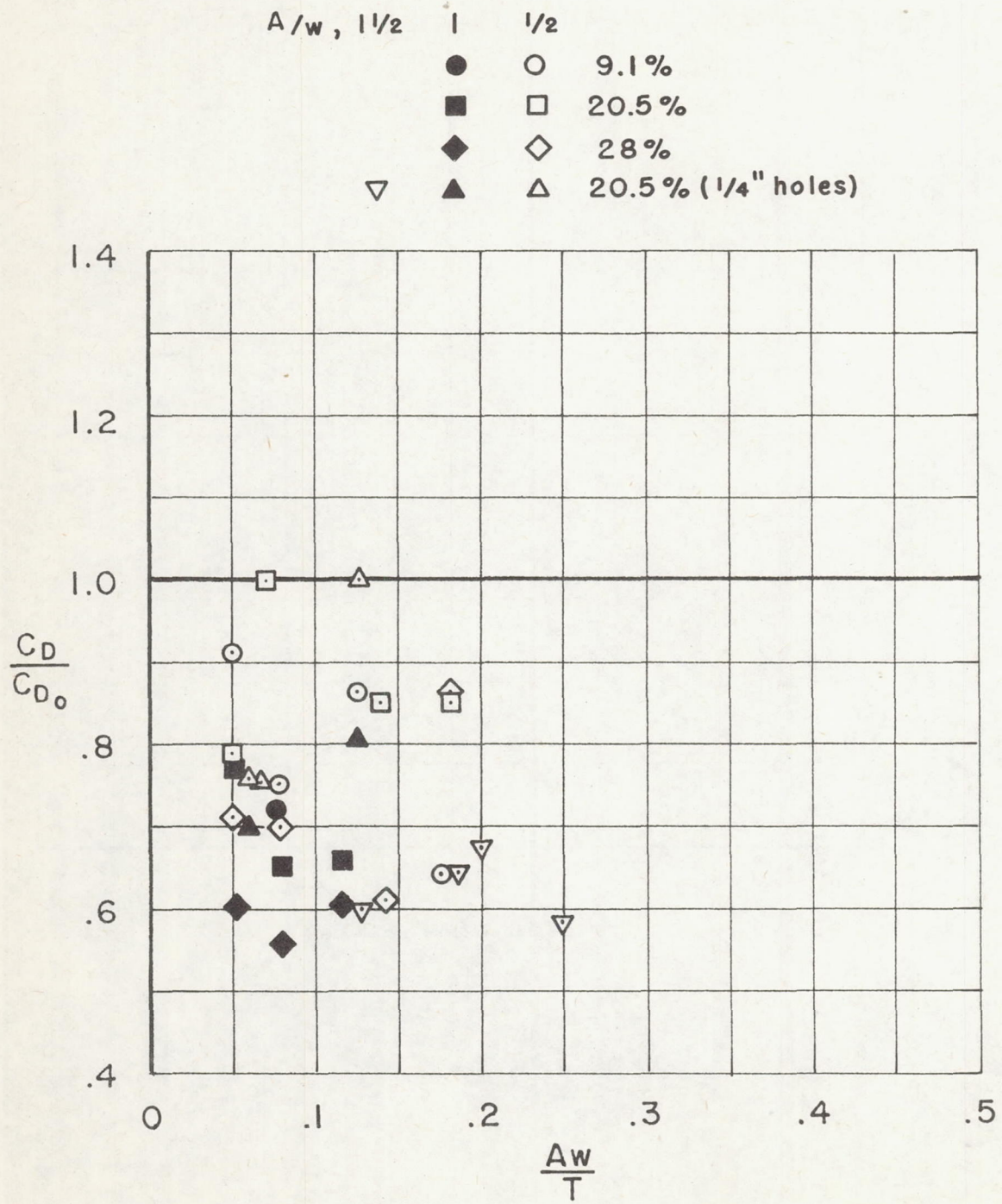


Figure 10.- Ratio of drag coefficient of baffle with cutouts to drag coefficient of baffle without cutouts.

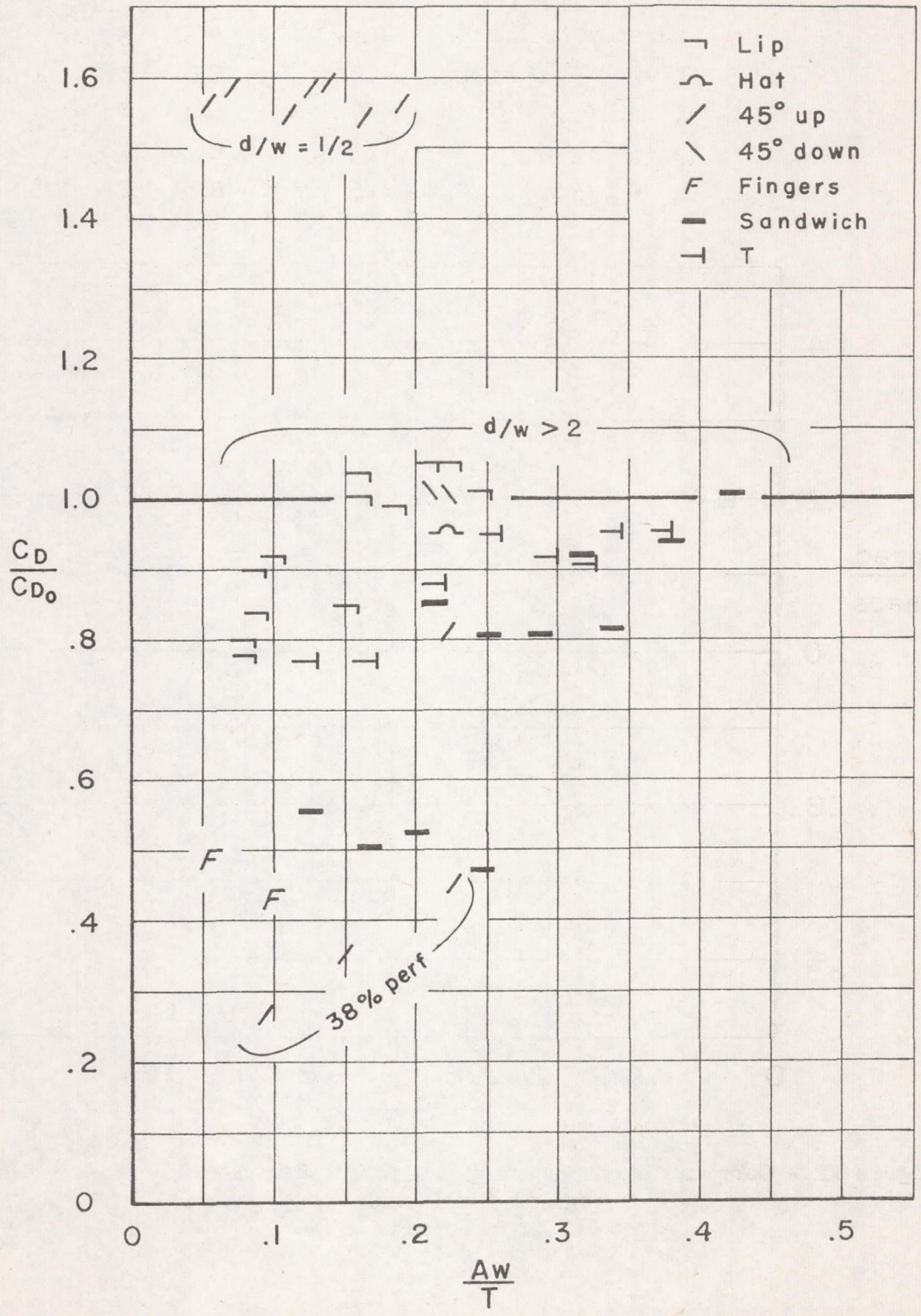


Figure 11.- Ratio of drag coefficient of shaped baffle to drag coefficient of flat plate of equal chord.

| Configuration | A/w | d/w | $\omega_n$ | w |
|---|---|---|---|---|
| ○ 45° Perf. ring | .5 | .4 | 3.6 | .58 |
| □ Ring | .9 | 5 | 6.3 | .13 |
| ◇ Ring | 1.5 | 2 | 6.3 | .13 |
| △ Ring | .5 | 2.5 | 6.3 | .25 |

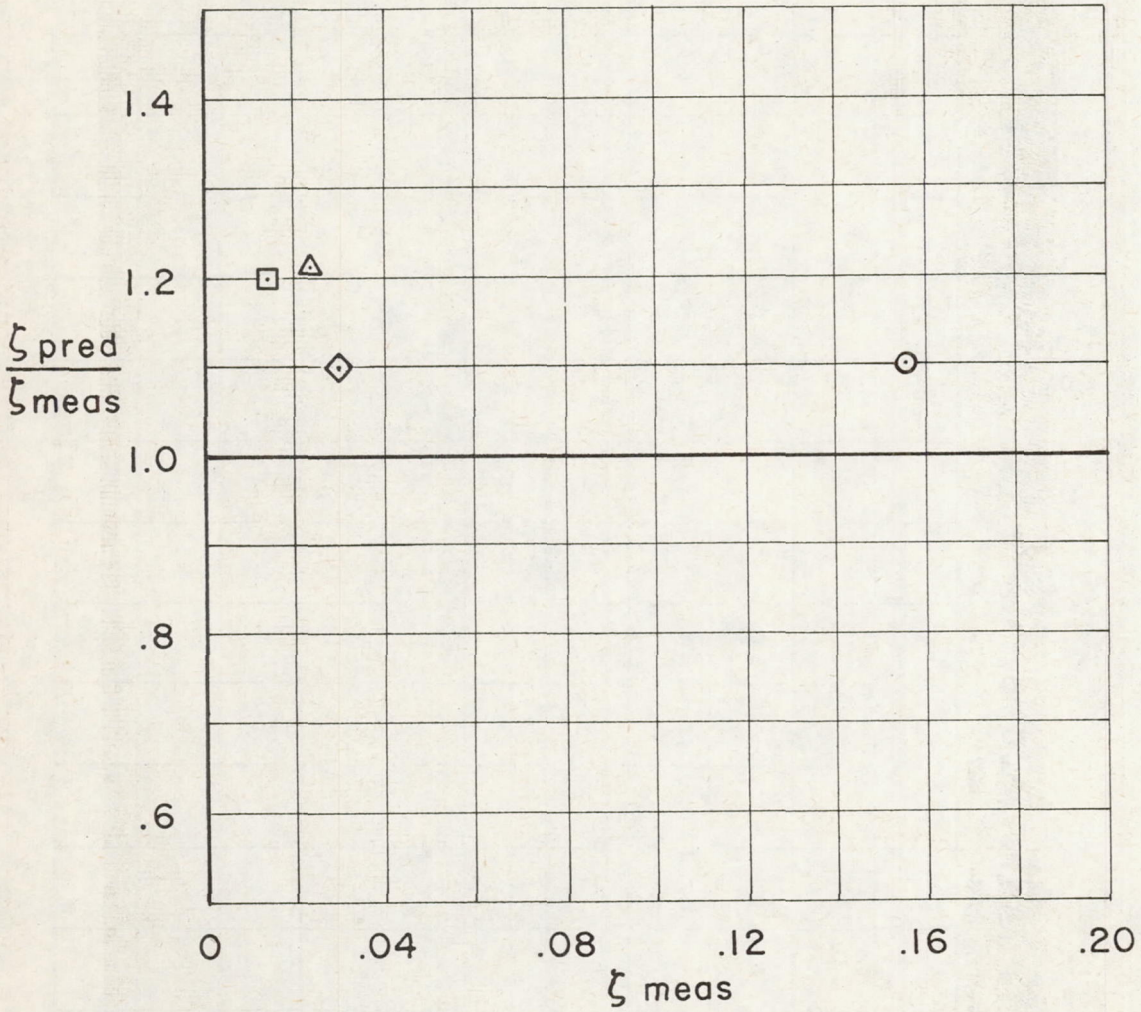




Figure 12.- Correlation of damping predicted with damping measured in cylindrical tanks.

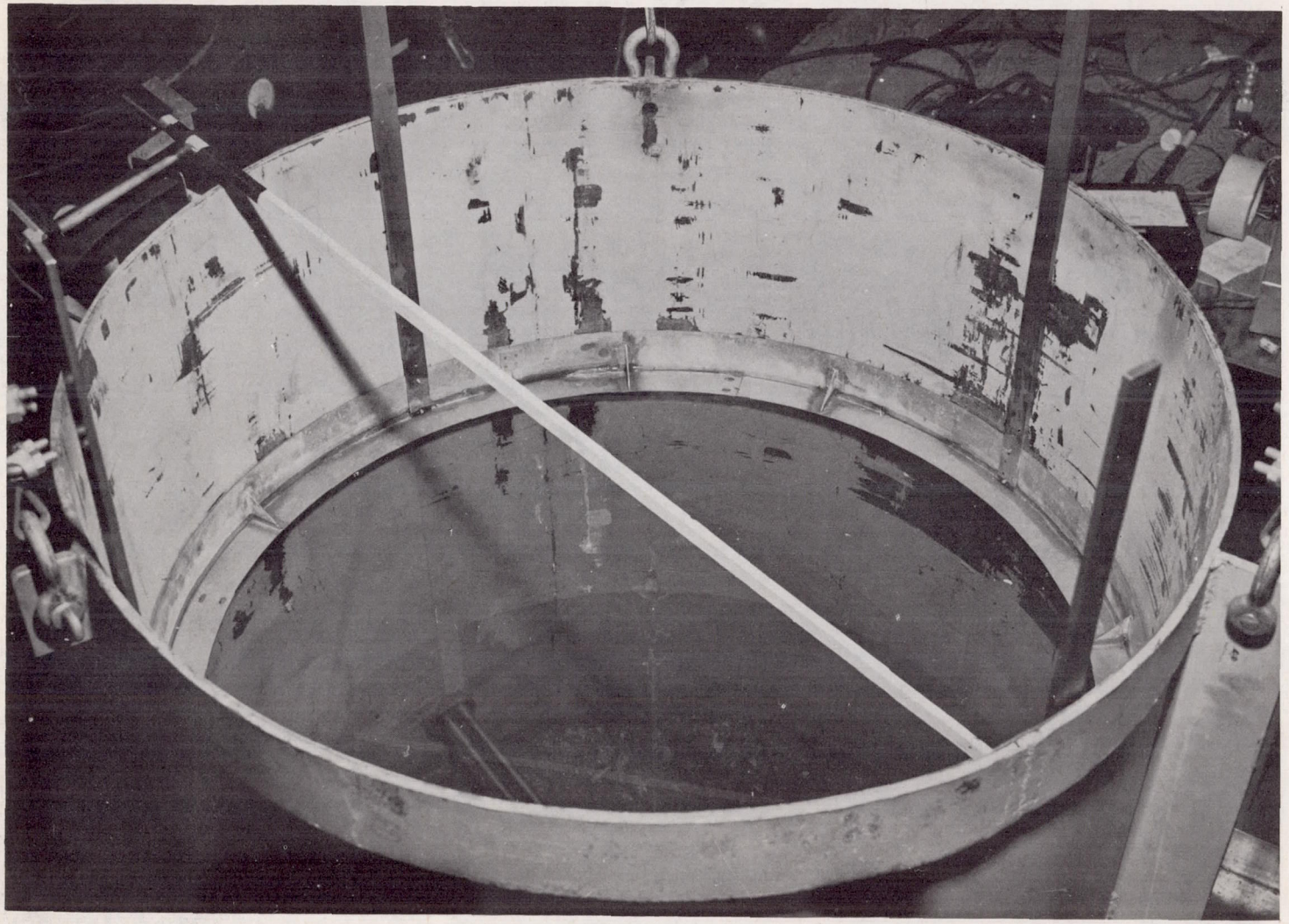

(a) 1-1/2-inch ring. A-26505

Figure 13.- Three-dimensional baffle configurations.

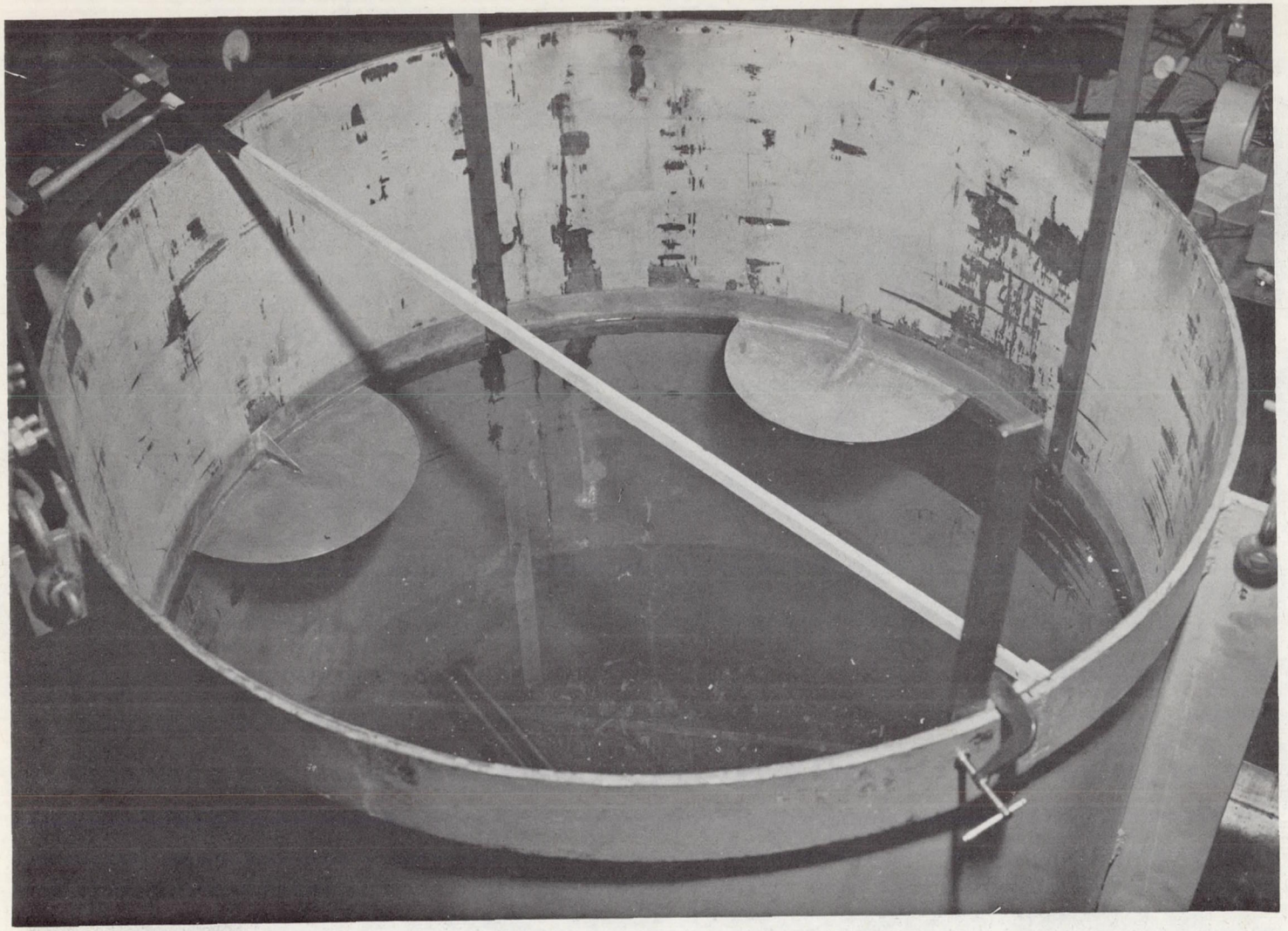

(b) Semicircular plates. A-26506

Figure 13.- Continued.

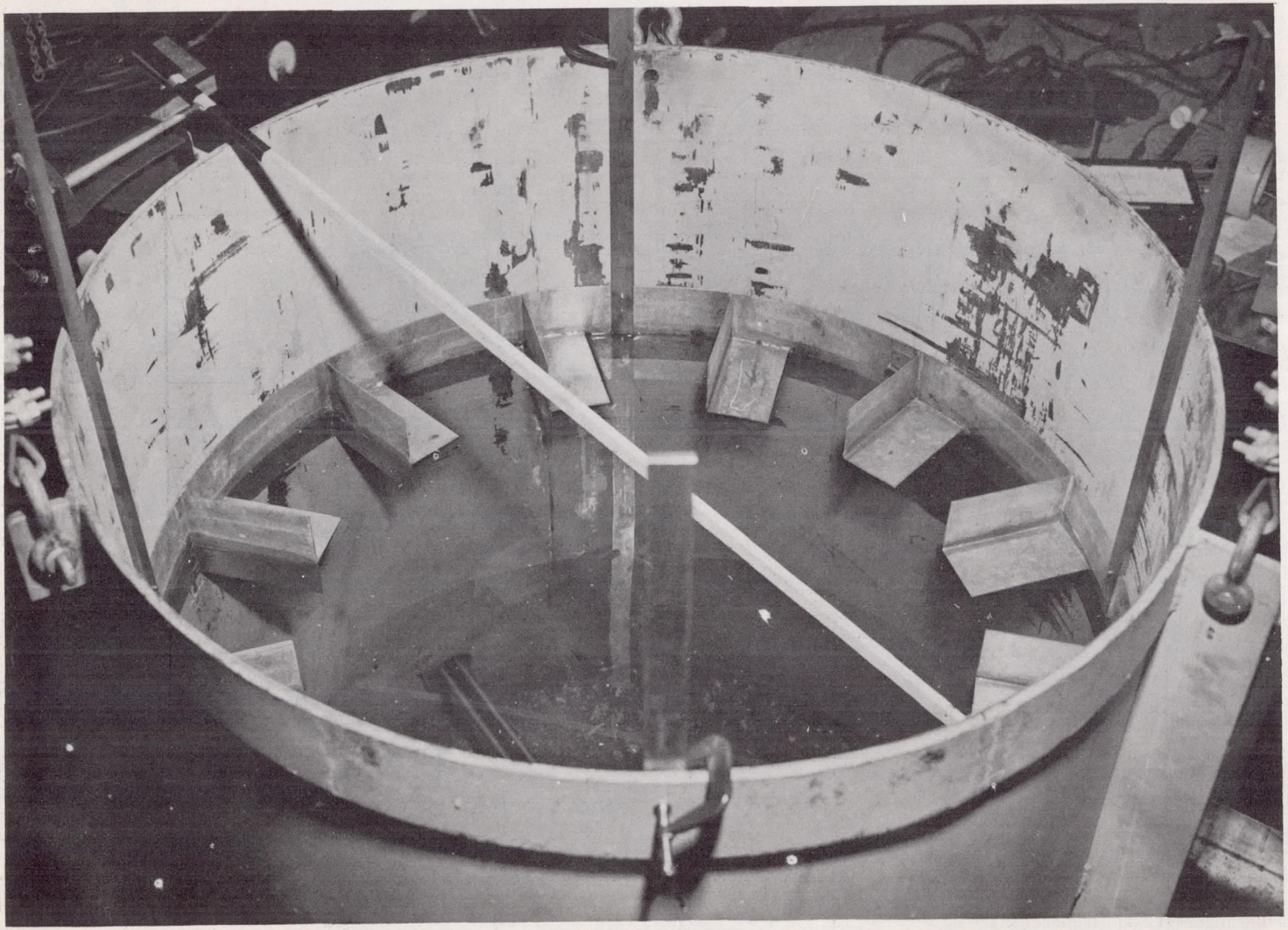

(c) Swirl plates. A-26508

Figure 13.- Concluded.

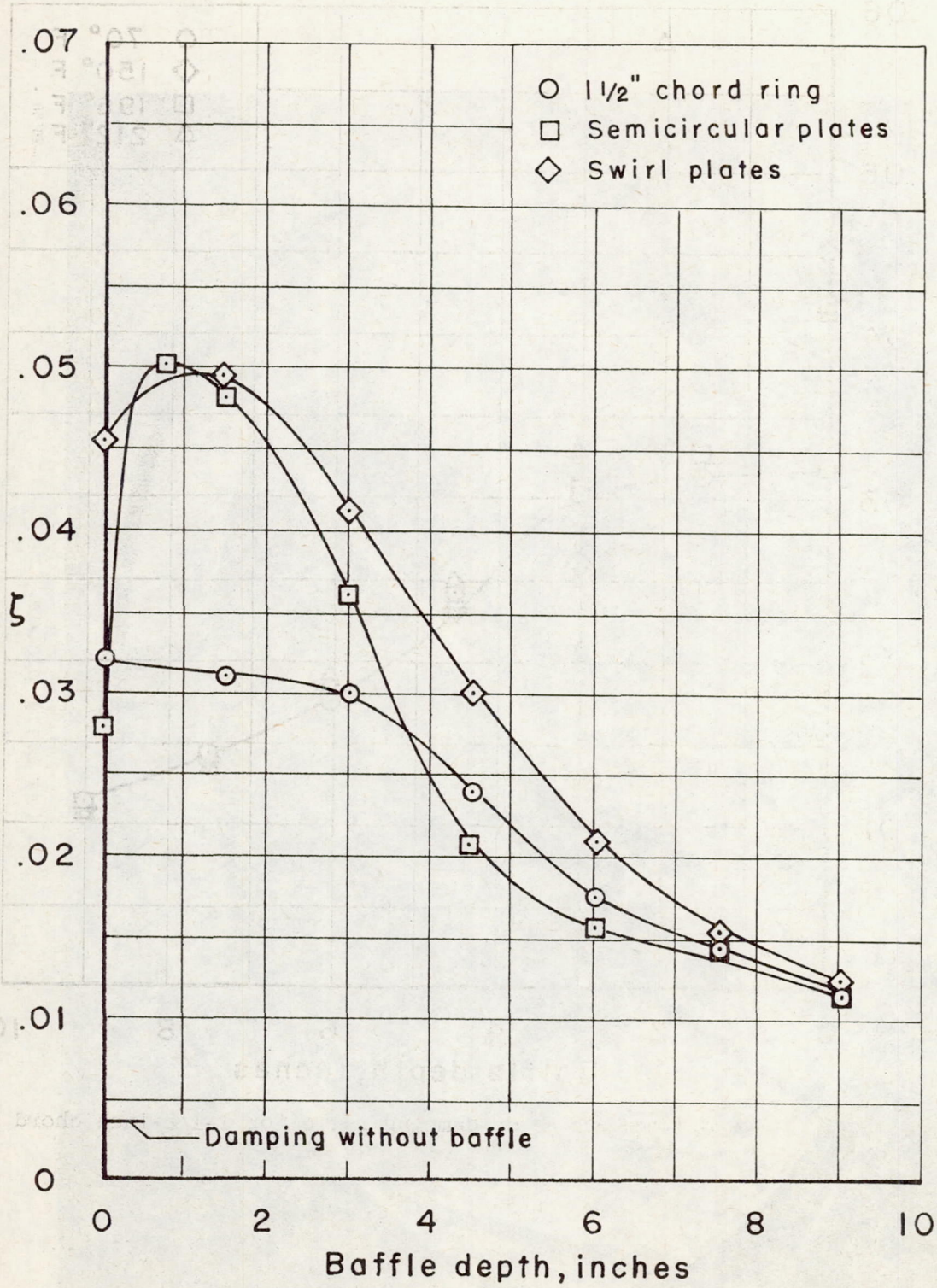


Figure 14.- Damping ratio of free-free tank with various baffles based on decaying oscillation at surface double amplitude of 3 inches.

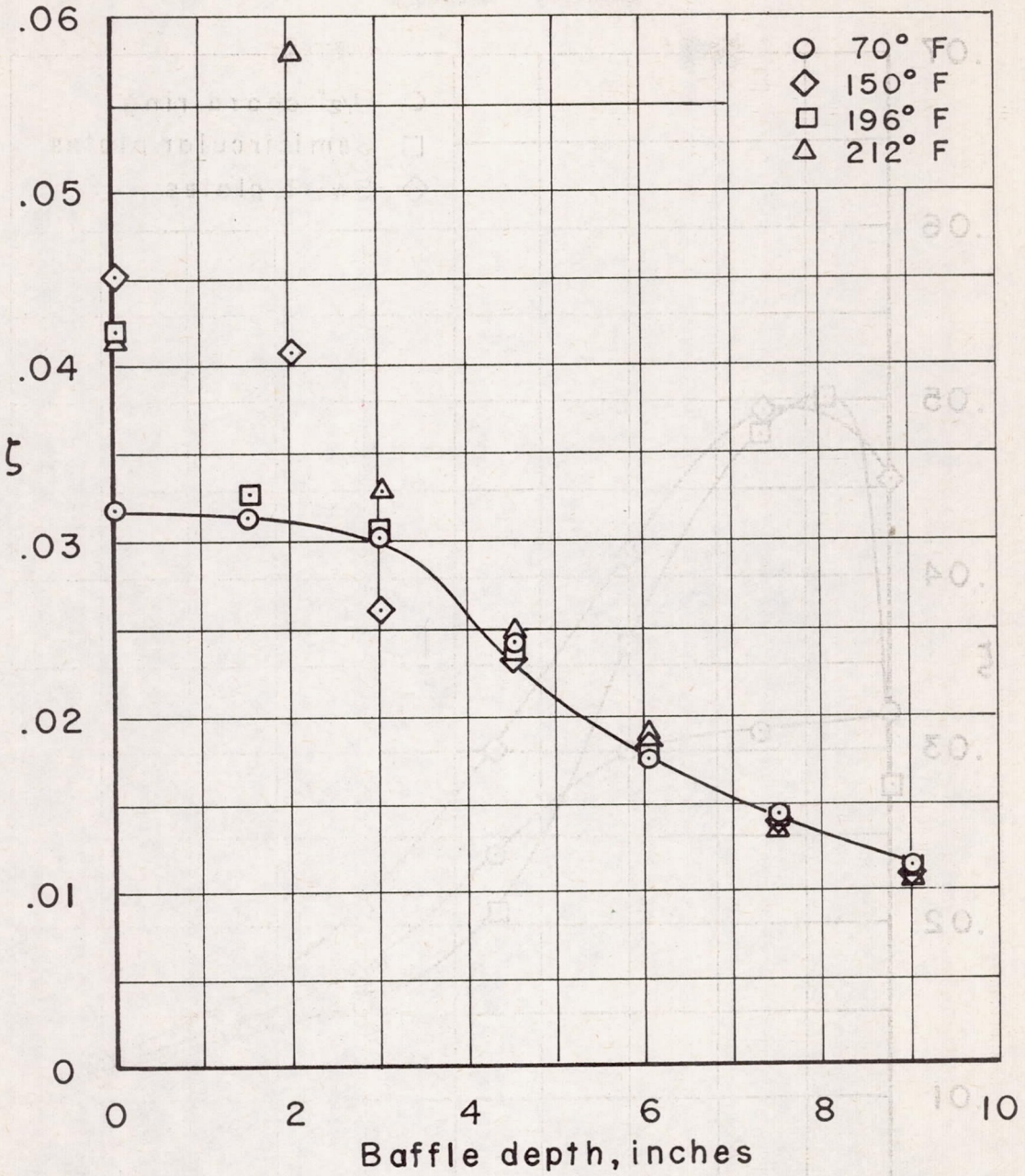


Figure 15.- Effect of temperature on damping ratio for 1-1/2-inch chord ring.